

Short-range and tensor correlations in ${}^4\text{He}$ and ${}^8\text{Be}$ studied with antisymmetrized quasi cluster model

N. Itagaki

*Yukawa Institute for Theoretical Physics, Kyoto University,
Kitashirakawa Oiwake-Cho, Kyoto 606-8502, Japan*

H. Matsuno, Y. Kanada-En'yo

Department of Physics, Kyoto University, Kitashirakawa Oiwake-Cho, Kyoto 606-8502, Japan

We apply tensor version of antisymmetrized quasi cluster model (AQCM-T) to ${}^4\text{He}$ and ${}^8\text{Be}$ while focusing on the NN correlations in α clusters. We adopt the NN interactions including realistic ones containing a repulsive core for the central part in addition to the tensor part. In ${}^4\text{He}$, the pn pair in the 3D channel has been known to play a decisive role in the tensor correlation and the framework is capable of treating not only this channel but also the NN correlations in the 1S and 3S channels. In ${}^8\text{Be}$, when two α clusters approach, the 3D pair is suppressed because of the Pauli blocking effect, which induces the decrease of the 3S component through the 3S - 3D coupling. This effect results in the reduction of the attractive effect of the central-even interaction in the middle-range region.

I. INTRODUCTION

The ${}^4\text{He}$ nucleus is a strongly bound many-nucleon system in the light mass region, thus the α clusters can be basic building blocks of the nuclear structure. The α cluster models [1, 2] have been developed and applied in numerous works for the description of cluster structures such as 3α clustering in the so-called Hoyle state of ${}^{12}\text{C}$ [3–5]. In most of the conventional cluster models, however, each α cluster is assumed as a simple $(0s)^4$ configuration, which is spin singlet, and therefore the contributions of non-central interactions, the spin-orbit and tensor interactions, completely vanish even though they play crucial roles in the nuclear structure [6–8]. Also, nucleons are correlated owing to the repulsive core in the short-range part of the central interaction, and this effect is not explicitly treated in the conventional structure models including cluster models. These days, such NN correlation is widely discussed based on modern *ab initio* theories not only in very light nuclei but also in medium-heavy nuclei [9–13]. Moreover, there are many experimental attempts with deep inelastic scattering to pin down the NN correlations in nuclei in wide mass number regions (see for example, Refs. [12, 14] and references therein). In study of cluster aspects in nuclear systems, it is an urgent issue to extend the model space and take into account these higher correlations beyond the $(0s)^4$ configuration in the cluster model.

Concerning the non-central interactions, recently, many attempts of directly taking into account them for the microscopic studies of cluster structure have begun; antisymmetrized molecular dynamics (AMD) [15–18], its extended version [19], and Fermionic molecular dynamics (FMD) [20–22] combined with the unitary correlation method (UCOM). In UCOM, the effects of non-central interaction and also short-range correlation are included with the unitary transformation of the Hamiltonian, which in principle induces many-body operators

up to A (mass number) body.

Our aim is to introduce an effective model, which is phenomenological but capable of directly taking into account the non-central interactions in a simplified manner without transforming the Hamiltonian. Concerning the rank one non-central interaction, the spin-orbit interaction, we proposed the antisymmetrized quasi cluster model (AQCM) [23–34]. By introducing a parameter for the imaginary part of the Gaussian centroids of single-particle wave functions in α clusters, we can smoothly transform α clusters to jj -coupling shell model wave functions, where the transformed α clusters contains cluster breaking components and are called quasi clusters.

Recently, the imaginary centered Gaussian wave packets have been utilized to directly take into account the rank two non-central interaction, tensor interaction [35–37]. In the previous paper [38], we newly proposed AQCM-T, which is an improved version of AQCM so as to explicitly treat the tensor correlation in the two-nucleon pairs. It has been known that the pn pair in the 3D channel plays a decisive role in the tensor correlation and this new framework is capable of treating not only this channel but also the NN correlations in the 1S and 3S channels in a very simplified way. The AQCM-T model with the new interaction was applied to ${}^8\text{Be}$, where the relation between the α - α cluster structure and the tensor interaction has been discussed. It was found that the tensor suppression gives a significant contribution to the α - α repulsion at short distances consistently with the pioneering works [39–41].

In the present study, we aim to describe the short-range correlation caused by the repulsive core of the central interaction in addition to the tensor correlation; we apply AQCM-T to ${}^4\text{He}$ and ${}^8\text{Be}$ using a realistic NN interaction containing a repulsive core for the central part. We focus on the NN correlations in α clusters. This paper is organized as follows; in Sec. II, the framework,

especially for the model wave function, is explained. In Sec. III, the Hamiltonian of the present model is described. In sections IV and V, the numerical results for ${}^4\text{He}$ and ${}^4\text{Be}$ are presented, respectively. The summary is presented in Sec. VI.

II. FORMULATIONS

In the present study, we aim to describe the short-range correlation caused by the repulsive core of the central interaction in addition to the tensor correlation; we apply AQCM-T to ${}^4\text{He}$ and ${}^8\text{Be}$ using a realistic NN interaction containing a repulsive core for the central part. The procedures of the calculation based on AQCM-T is, in principle, the same as those presented in the previous paper [38], and the readers can refer to it for the detailed formulations. Here we first explain the AQCM-T treatment for a single NN -pair, which are correlated, and next give the formulation of AQCM for actual nuclei, ${}^4\text{He}$ and ${}^8\text{Be}$.

A. AQCM-T for a NN -pair

Each single-particle wave function is written by Gaussian wave packet as

$$\psi_j(i) = \phi_{\mathbf{S}_j}(\mathbf{r}_i) \chi_j(s_i, \tau_i), \quad (1)$$

$$\phi_{\mathbf{S}_j}(\mathbf{r}_i) = \left(\frac{2\nu}{\pi}\right)^{\frac{3}{4}} e^{-\nu(\mathbf{r}_i - \mathbf{S}_j)^2}, \quad (2)$$

where \mathbf{S}_j ($j = 1, 2$) is the Gaussian centroid and χ_j is the spin-isospin wave function. The width parameter ν is set to $\nu = 0.25 \text{ fm}^{-2}$ and fixed in all calculations of this paper.

For Gaussian centroids of two nucleons in a correlated NN -pair, we adopt the following complex conjugate values,

$$\begin{aligned} \mathbf{S}_1 &= \mathbf{R} + \frac{i\mathbf{K}}{\nu} = \mathbf{R} + \frac{i\mathbf{k}}{2\nu}, \\ \mathbf{S}_2 &= \mathbf{R} - \frac{i\mathbf{K}}{\nu} = \mathbf{R} - \frac{i\mathbf{k}}{2\nu}, \end{aligned} \quad (3)$$

where \mathbf{R} and \mathbf{K} are real vectors, and $\mathbf{k} \equiv 2\mathbf{K}$. The NN -pair wave function can be written in a separated form for the relative and center of mass (cm) coordinates, $\mathbf{r} = \mathbf{r}_1 - \mathbf{r}_2$ and $\mathbf{r}_g = (\mathbf{r}_1 + \mathbf{r}_2)/2$, respectively, as

$$\phi_{\mathbf{S}_1}(\mathbf{r}_1) \phi_{\mathbf{S}_2}(\mathbf{r}_2) = \varphi_{\mathbf{k}}(\mathbf{r}) \phi_g(\mathbf{r}_g), \quad (4)$$

$$\varphi_{\mathbf{k}}(\mathbf{r}) = \left(\frac{\nu}{\pi}\right)^{\frac{3}{4}} e^{-\frac{\nu}{2}r^2 + i\mathbf{k}\cdot\mathbf{r} + \frac{k^2}{2\nu}}, \quad (5)$$

$$\phi_g(\mathbf{r}_g) = \left(\frac{4\nu}{\pi}\right)^{\frac{3}{4}} e^{-2\nu(\mathbf{r}_g - \mathbf{R})^2}. \quad (6)$$

The expectation values of the positions and momenta of the relative and cm coordinates are given as

$$\langle \hat{\mathbf{r}} \rangle = 0, \quad \langle \hat{\mathbf{p}} \rangle = \mathbf{k}, \quad (7)$$

$$\langle \hat{\mathbf{r}}_g \rangle = \mathbf{R}, \quad \langle \hat{\mathbf{p}}_g \rangle = 0. \quad (8)$$

Note that the Fourier components of the relative wave function $\varphi_{\mathbf{k}}(\mathbf{r})$ also has a Gaussian form, which is localized at \mathbf{k} with the dispersion of $\sqrt{\nu}$. As shown in Ref. [36], the relative wave function for a non-zero vector \mathbf{k} contain various partial-wave components as

$$\begin{aligned} \varphi_{\mathbf{k}}(\mathbf{r}) &= 4\pi \left(\frac{\nu}{\pi}\right)^{\frac{3}{4}} e^{-\frac{\nu}{2}r^2 + \frac{k^2}{2\nu}} \\ &\times \sum_{lm} i^l j_l(kr) Y_{lm}(\mathbf{e}_k) Y_{lm}(\mathbf{e}_r). \end{aligned} \quad (9)$$

In order to take into account the tensor coupling between 3D and 3S channels of the $T = 0$ NN -pair, we project the NN -pair onto the positive-parity state and set \mathbf{k} along the z axis as $\mathbf{k} = (0, 0, k)$ as done in the previous paper [38]. Then the relative wave function can be expressed as

$$\begin{aligned} \varphi_{\mathbf{k}}^+(\mathbf{r}) &= \left(\frac{\nu}{\pi}\right)^{\frac{3}{4}} e^{-\frac{\nu}{2}r^2 + \frac{k^2}{2\nu}} \cos(kz) \\ &= \left(\frac{\nu}{\pi}\right)^{\frac{3}{4}} e^{-\frac{\nu}{2}r^2 + \frac{k^2}{2\nu}} 4\pi \sum_{l=\text{even}} \sqrt{\frac{2l+1}{4\pi}} i^l j_l(kr) Y_{l0}(\mathbf{e}_r) \\ &= \sum_{l=\text{even}} a_l \varphi_k^{(l)}(r) Y_{l0}(\mathbf{e}_r), \end{aligned} \quad (10)$$

where a_l is the normalization factor, and $\varphi_k^{(l)}(r)$ is the normalized radial wave function of the l -even basis state proportional to $e^{-\frac{\nu}{2}r^2} j_l(kr)$.

B. AQCM-T for ${}^4\text{He}$

Next, we apply the NN -pair wave function described in the previous subsection to the two correlating nucleons in ${}^4\text{He}$.

1. Model wave function of ${}^4\text{He}$

For the ${}^4\text{He}$ system, in addition to the correlated NN -pair described by AQCM-T, we consider a $(0s)^2$ (uncorrelated) pair, and both pairs are placed at the origin. The AQCM-T wave function for ${}^4\text{He}$ is expressed as

$$\begin{aligned} \Phi_{{}^4\text{He}, 0^+}^{\text{AQCM-T}} &= \hat{P}^{0+} \mathcal{A} \{ \phi_{\frac{i\mathbf{k}}{2\nu}} \chi_1 \phi_{-\frac{i\mathbf{k}}{2\nu}} \chi_2, \phi_0 \chi_3, \phi_0 \chi_4 \} \\ &= \hat{P}^{0+} \mathcal{A} \{ \phi_{\frac{i\mathbf{k}}{2\nu}} \phi_{-\frac{i\mathbf{k}}{2\nu}} \phi_0 \phi_0 \otimes \chi_1 \chi_2 \chi_3 \chi_4 \}, \end{aligned} \quad (11)$$

where \mathcal{A} is the antisymmetrizer for all the nucleons, \hat{P}^{0+} is the projection operator to $J^\pi = 0^+$ (in practice numerically performed), and $\phi_0 = \phi_{\mathbf{S}=0}$ is the spatial wave

function for a nucleon in the $0s$ orbit. The spatial wave function of the total system in the intrinsic frame before the projections is rewritten as

$$\phi_{\frac{i\mathbf{k}}{2\nu}}\phi_{-\frac{i\mathbf{k}}{2\nu}}\phi_0\phi_0 = \phi_g(\mathbf{r}_g)\phi_g(\mathbf{r}'_g)\varphi_{\mathbf{k}}(\mathbf{r})\varphi_0(\mathbf{r}'), \quad (12)$$

$$\mathbf{r}_g = \frac{\mathbf{r}_1 + \mathbf{r}_2}{2}, \quad \mathbf{r}'_g = \frac{\mathbf{r}_3 + \mathbf{r}_4}{2}, \quad (13)$$

$$\mathbf{r} = \mathbf{r}_1 - \mathbf{r}_2, \quad \mathbf{r}' = \mathbf{r}_3 - \mathbf{r}_4, \quad (14)$$

where \mathbf{r} and \mathbf{r}_g (\mathbf{r}' and \mathbf{r}'_g) are the relative and cm coordinates of the pair, respectively. The NN correlation is taken into account through $\varphi_{\mathbf{k}}(\mathbf{r})$ in the case of the correlated NN -pair.

For the choice of the spin-isospin configurations, one should care about the redundancies originating from the parity and angular momentum projections as well as the Fermi statistics (antisymmetrization effect). For the $J^\pi = 0^+$ states of ${}^4\text{He}$, the model space for a given k value ($k \neq 0$) contains only the S -wave ($\varphi_k^{(0)}$) and D -wave ($\varphi_k^{(2)}$) components, which are coupled to the total intrinsic spin $S = 0$ and $S = 2$ of the four nucleons, respectively. For the 0^+ state with the $\mathbf{k} = (0, 0, k)$ choice, only the $S_z = 0$ states contribute, and in total we have five independent spin and isospin configurations;

$$\begin{aligned} \chi_1\chi_2\chi_3\chi_4 = \\ \{p \uparrow p \downarrow n \uparrow n \downarrow, \quad n \uparrow n \downarrow p \uparrow p \downarrow, \\ p \uparrow n \uparrow p \downarrow n \downarrow, \quad p \uparrow n \downarrow p \uparrow n \downarrow, \\ p \uparrow n \downarrow p \downarrow n \uparrow\}. \end{aligned} \quad (15)$$

Furthermore, when we ignore small breaking of the isospin symmetry by the Coulomb interaction, the five configurations in Eq. (15) can be reduced into three channels with respect to spin and isospin symmetries of the NN -pair as

$$\begin{aligned} {}^1S: \quad & \phi_g(\mathbf{r}_g)\phi_g(\mathbf{r}'_g) \otimes \varphi_k^{(0)}(r)\varphi_0^{(0)}(r') \\ & \otimes Y_{00}(\mathbf{e}_r)Y_{00}(\mathbf{e}_{r'}) \otimes \chi_0^\sigma\chi_0^\sigma \otimes [\chi_1^\tau\chi_1^\tau]_{T=0}, \end{aligned} \quad (16)$$

$$\begin{aligned} {}^3S: \quad & \phi_g(\mathbf{r}_g)\phi_g(\mathbf{r}'_g) \otimes \varphi_k^{(0)}(r)\varphi_0^{(0)}(r') \\ & \otimes Y_{00}(\mathbf{e}_r)Y_{00}(\mathbf{e}_{r'}) \otimes [\chi_1^\sigma\chi_1^\sigma]_{S=0} \otimes \chi_0^\tau\chi_0^\tau, \end{aligned} \quad (17)$$

$$\begin{aligned} {}^3D: \quad & \phi_g(\mathbf{r}_g)\phi_g(\mathbf{r}'_g) \otimes \varphi_k^{(2)}(r)\varphi_0^{(0)}(r') \\ & \otimes [Y_{20}(\mathbf{e}_r)Y_{00}(\mathbf{e}_{r'}) \otimes [\chi_1^\tau\chi_1^\tau]_{S=2}]_{J=0} \otimes \chi_0^\tau\chi_0^\tau, \end{aligned} \quad (18)$$

where $\chi_{0,1}^\sigma$ ($\chi_{1,0}^\tau$) is the spin (isospin) function of the NN -pairs coupled to the spin (isospin) singlet and triplet states, respectively. Note that $\varphi_0^{(0)}$ ($= \varphi_{k=0}^{(0)}$) expresses the uncorrelated NN -pair with the $(0s)^2$ configuration. The first (second) configuration takes into account the NN correlation in the 1S (3S) channel and is essential for the short-range correlation caused by the repulsive core of the central interaction. The third configuration is the so-called D -state component and contributes to the

tensor correlation. We call the first, second, and third configurations, the 1S , 3S , and 3D channels, respectively.

If the charge symmetry breaking by the Coulomb interaction can be ignored, the three-channel (1S , 3S , and 3D) calculation is equivalent to the configuration mixing of the five configurations defined in Eq. (15). Indeed, in the practical calculation of ${}^4\text{He}$, we found that almost equivalent results are obtained in two cases indicating that the charge symmetry breaking is negligibly small.

In the present framework, $\Phi_{{}^4\text{He},0^+}^{\text{AQCM-T}}$ defined in Eqs. (11) and (12) is a basis wave function specified by the momentum parameter k in $\mathbf{k} = (0, 0, k)$ and the channel $\beta = \{{}^1S, {}^3S, \text{ and } {}^3D\}$. The total wave function for the ground state, $\Psi_{{}^4\text{He,g.s.}}$, is therefore expressed by linear combination of various k values and the spin and isospin configurations as

$$\Psi_{{}^4\text{He,g.s.}} = c_0\Phi_{{}^4\text{He}}^{0s} + \sum_k \sum_\beta c(k, \beta)\Phi_{{}^4\text{He},0^+}^{\text{AQCM-T}}(k, \beta). \quad (19)$$

Here, $\Phi_{{}^4\text{He}}^{0s}$ in the first term is the $(0s)^4$ wave function, which is equivalent to the $k = 0$ AQCM-T wave function with $\beta = {}^1S$ or $\beta = {}^3S$. The coefficients c_0 and $c(k, \beta)$ are determined by diagonalizing the norm and Hamiltonian matrices comprised of the basis wave functions. The superposition of k in Eq. (19) is nothing but the expansion of the relative wave function of the correlated NN -pair in the momentum space with localized Gaussians at the mean momentum \mathbf{k} , and that of $\beta = \{{}^1S, {}^3S, \text{ and } {}^3D\}$ corresponds to the coupled-channel calculation of the three channels.

We explicitly treat the NN correlations of only a single NN -pair among the four nucleons but omit higher-order correlations, where more than two nucleons are involved. This ansatz is supported by the four-body calculation of ${}^4\text{He}$ by Horii *et al.* in Ref. [42] showing that the 3S - 3D coupling in a single NN -pair with $T = 0$ is essential to describe the tensor correlation in the ground state. However, this ansatz may not hold in the case of extremely hard core at the short-range region of the central interaction, which may promote the non-negligible amount of higher-order effects. To include higher-order correlations, recently, Myo *et al.* has proposed further improved framework with finite imaginary parts for the Gaussian centroids [37]. However, one of the advantages of the present AQCM-T model is that one can analyze the contribution and pair wave function in each of the three (1S , 3S , and 3D) channels because the ${}^4\text{He}$ wave function is explicitly expressed based on the spin-isospin symmetry of the two NN -pairs in the present model.

2. Parameter settings for ${}^4\text{He}$

For the ground state of ${}^4\text{He}$ (${}^4\text{He}(\text{g.s.})$), we perform calculations with the three channels ($\beta = \{{}^1S, {}^3S, {}^3D\}$). For each channel, the basis states with $k = 0.5, 1.0, \dots, 5.5 \text{ fm}^{-1}$ (11 states) are adopted in ad-

dition to the $(0s)^4$ configuration. We also perform truncated calculations by selecting parameters k and/or channels β to clarify the roles of high momentum components in each 1S , 3S , and 3D channel.

C. AQCM-T for ^8Be

1. Basis wave function for two- α system

Our aim is to investigate effects of the NN correlations in heavier nuclei. Here we extend the AQCM-T framework to ^8Be with a two- α cluster structure, in which one of α clusters is changed from the $(0s)^4$ configuration to the correlated ^4He wave function previously explained. We label the correlated α cluster as α_k , and another α cluster with the $(0s)^4$ configuration is labeled as α_0 . We place α_k at $\mathbf{R} = \frac{\mathbf{d}}{2}$ and α_0 at $\mathbf{R}' = -\frac{\mathbf{d}}{2}$ with the relative distance of $d \equiv |\mathbf{d}|$. After the antisymmetrization, the two- α wave function projected to 0^+ is

$$\Phi_{2\alpha,0^+}^{\text{AQCM-T}}(k, \beta, \mathbf{d}) = \widehat{P}^{0+} \mathcal{A} \{ \Phi_{\alpha_k}(k, \beta, \mathbf{R}) \Phi_{\alpha_0}(\mathbf{R}') \}, \quad (20)$$

where k and β are the momentum parameter and the channel of the α_k cluster. The α_k and α_0 clusters are expressed using the AQCM-T wave function for ^4He as

$$\begin{aligned} \Phi_{\alpha_k}(k, \beta, \mathbf{R}) &= \Phi_{^4\text{He},+}^{\text{AQCM-T}}(k, \beta, \mathbf{R}) \\ &= \frac{1 + \widehat{P}_k}{2} \mathcal{A} \{ \phi_{\mathbf{R} + \frac{i\mathbf{k}}{2\nu}} \phi_{\mathbf{R} - \frac{i\mathbf{k}}{2\nu}} \phi_{\mathbf{R}} \phi_{\mathbf{R}} \otimes \chi_1 \chi_2 \chi_3 \chi_4 \}, \quad (21) \\ \Phi_{\alpha_0}(\mathbf{R}') &= \Phi_{^4\text{He}}^{0s}(\mathbf{R}') \\ &= \mathcal{A} \{ \phi_{\mathbf{R}'} \phi_{\mathbf{R}'} \phi_{\mathbf{R}'} \phi_{\mathbf{R}'} \otimes p \uparrow p \downarrow n \uparrow n \downarrow \}. \quad (22) \end{aligned}$$

Here $\mathbf{k} = (0, 0, k)$, and the operator \widehat{P}_k transforms the imaginary part of the correlated NN -pair as $k \rightarrow -k$, and $(1 + \widehat{P}_k)/2$ corresponds to the intrinsic parity projection of the correlated NN -pair in the α_k cluster. Here, \mathbf{d} is chosen as $\mathbf{d} = (d \sin \theta_\alpha, 0, d \cos \theta_\alpha)$, where d and θ_α stands for the distance and angle of the relative position between the two α clusters.

2. Full GCM calculation for two- α system

Based on the generator coordinate method (GCM), all the AQCM-T wave function with various k , θ_α , β , and d values are superposed as

$$\begin{aligned} \Psi_{2\alpha,0^+}^{\text{GCM}} &= \sum_d \left[c_0(d) \Phi_{2\alpha,0^+}^{0s}(d) \right. \\ &\left. + \sum_{k,\beta,\theta_\alpha} c(k, \beta, \theta_\alpha, d) \Phi_{2\alpha,0^+}^{\text{AQCM-T}}(k, \beta, \mathbf{d}) \right], \quad (23) \end{aligned}$$

where $\Phi_{2\alpha,0^+}^{0s}$ is the $(0s)^4$ - $(0s)^4$ state with the distance d given by the Brink-Bloch (BB) wave function projected onto $J^\pi = 0^+$ as,

$$\Phi_{2\alpha,0^+}^{0s}(d) = \widehat{P}^{0+} \mathcal{A} \{ \Phi_{\alpha_0}(\mathbf{R}) \Phi_{\alpha_0}(\mathbf{R}') \}. \quad (24)$$

In Eq. (23), the coefficients $c_0(d)$ and $c(k, \beta, \theta_\alpha, d)$ are determined by diagonalizing the norm and Hamiltonian matrices. This is called full GCM calculation.

In addition to k and β of the correlated NN -pair in α_k , the inter-cluster motion is described with the distance parameter d and the angular parameter θ_α . It should be noted that the intrinsic wave function of α_k is axial symmetric and positive-parity state, and that for the α_0 is rotationally invariant, thus the angular range of $0 \leq \theta_\alpha \leq \pi/2$ is enough.

3. Fixed- d calculation

In order to see properties of the two- α system as a function of the inter-cluster distance d , we also show results with fixed value of d called ‘‘fixed- d calculation’’,

$$\begin{aligned} \Psi_{2\alpha,0^+}^{\text{opt}}(d) &= f_0^d \Phi_{2\alpha,0^+}^{0s}(d) \\ &+ \sum_{k,\beta,\theta_\alpha} f^d(k, \beta, \theta_\alpha) \Phi_{2\alpha,0^+}^{\text{AQCM-T}}(k, \beta, \mathbf{d}). \quad (25) \end{aligned}$$

For each d value, the coefficients $\{f_0^d\}$ and $\{f^d(k, \beta, \theta_\alpha)\}$ are determined by diagonalizing the norm and Hamiltonian matrices. This means that the coefficients $\{f_0^d\}$ and $\{f^d\}$ are optimized so as to minimize the energy of the two- α system at each d ,

$$E^{\text{opt}}(d) = \langle \Psi_{2\alpha,0^+}^{\text{opt}}(d) | \widehat{H} | \Psi_{2\alpha,0^+}^{\text{opt}}(d) \rangle, \quad (26)$$

which corresponds to the adiabatic approximation. To stress the optimization of the α cluster at each d , we also call the fixed- d calculation ‘‘optimized- α ’’ calculation.

At large α - α distances, the two- α system approaches the asymptotic state, in which each α cluster stays in the ground state as isolated ^4He . This asymptotic state is approximately described by the fixed- d calculation with large enough d . As two α clusters approach each other, each α cluster is excited because of the Pauli blocking effect and potential energy effect from the other α cluster. The internal excitation of α clusters, which is usually called the core polarization, is taken into account by this fixed- d calculation in an adiabatic way.

4. Frozen- α calculation

We also show the energies of ‘‘frozen α -clusters’’, where the core polarization at short relative distances is omitted. We use the α clusters obtained at the largest distance of the model, $d = d_{\text{max}}$, for any value of d . Namely, the coefficients $f_0^{d_{\text{max}}}$ and $f^{d_{\text{max}}}(k, \beta, \theta_\alpha)$ are optimized at $d = d_{\text{max}}$ and they are used for any d as

$$\begin{aligned} \Psi_{2\alpha,0^+}^{\text{frozen}}(d) &= f_0^{d_{\text{max}}} \Phi_{2\alpha,0^+}^{0s}(d) \\ &+ \sum_{k,\beta,\theta_\alpha} f^{d_{\text{max}}}(k, \beta, \theta_\alpha) \Phi_{2\alpha,0^+}^{\text{AQCM-T}}(k, \beta, \mathbf{d}). \quad (27) \end{aligned}$$

The expectation values of the Hamiltonian at d is then

$$E^{\text{frozen}}(d) = \langle \Psi_{2\alpha,0^+}^{\text{frozen}}(d) | \hat{H} | \Psi_{2\alpha,0^+}^{\text{frozen}}(d) \rangle. \quad (28)$$

5. Internal and external energies

We also estimate the contribution from the internal excitation of α cluster (internal energy) and the residual part (external energy) at each distance d . The energy difference between the optimized energy at d and that at the largest distance of $d = d_{\text{max}}$ is defined as $E_r^{\text{opt}}(d) = E^{\text{opt}}(d) - E^{\text{opt}}(d_{\text{max}})$. Here $E_r^{\text{opt}}(d)$ contains not only the effect of the internal excitation due to the core polarization ($\Delta E^{\text{internal}}$) but also the external energy between clusters, which is interpreted as a kind of α - α potential where the internal excitation energy is excluded. This means that $E_r^{\text{opt}}(d)$ can be divided into two parts as

$$E_r^{\text{opt}}(d) = \Delta E^{\text{internal}}(d) + \Delta E^{\text{external}}(d). \quad (29)$$

We estimate the internal excitation energies $\Delta E^{\text{internal}}(d)$ as follows. We first perform the fixed- d calculation at d . Keeping the optimized coefficients at d (f_0^d and $f^d(k, \beta, \theta_\alpha)$), we change d to the largest value, $d = d_{\text{max}}$, as

$$\begin{aligned} \Psi_{2\alpha,0^+}^{\text{core-exc}}(d; d_{\text{max}}) &= f_0^d \Phi_{2\alpha,0^+}^{0s}(d_{\text{max}}) \\ &+ \sum_{k,\beta,\theta_\alpha} f^d(k, \beta, \theta_\alpha) \Phi_{2\alpha,0^+}^{\text{AQCMT}}(k, \beta, \mathbf{d}_{\text{max}}). \end{aligned} \quad (30)$$

The corresponding energy is

$$E^{\text{core-exc}}(d) = \langle \Psi_{2\alpha,0^+}^{\text{core-exc}}(d; d_{\text{max}}) | \hat{H} | \Psi_{2\alpha,0^+}^{\text{core-exc}}(d; d_{\text{max}}) \rangle. \quad (31)$$

In this $\Psi_{2\alpha,0^+}^{\text{core-exc}}(d; d_{\text{max}})$, two α clusters are located with a large relative distance, but it still contains the core-polarization effect. Therefore, the internal excitation energy due to the core-excitation can be evaluated by comparing it with the optimal energy at d_{max} as

$$\Delta E^{\text{internal}}(d) \equiv E^{\text{core-exc}}(d) - E^{\text{opt}}(d_{\text{max}}). \quad (32)$$

Then, we simply define the external energy as

$$\Delta E^{\text{external}}(d) \equiv E_r^{\text{opt}}(d) - \Delta E^{\text{internal}}(d). \quad (33)$$

6. Parameter setting for ${}^8\text{Be}$

When we calculate ${}^8\text{Be}$, we introduce truncated model spaces for each α cluster. As shown later, the results of the truncations reasonably reproduce the full calculation for ${}^4\text{He}$.

For the relative angle between the two α clusters, we adopt four mesh points of $\theta_\alpha = (\pi/8)i$ ($i = 1, \dots, 4$), which gives almost converged results. Although five

points of $\theta_\alpha = (\pi/8)i$ ($i = 0, \dots, 4$) were used in the previous paper [38], we omit $\theta_\alpha = 0$, which is less important, to reduce the computational cost. The energy difference of the calculations with and without $\theta_\alpha = 0$ is 0.03 MeV for the case of G3RS2-3R interaction at $d = 6$ fm.

For the α - α distance parameter d , eight values of $d = 1, 2, \dots, 8$ fm are adopted. This is bound state approximation and α clusters are artificially confined in the range of $d \leq d_{\text{max}} = 8$ fm. Here $d_{\text{max}} = 8$ fm is close to the position of the Coulomb barrier around $d \sim 7$ fm.

As a result, the number of states with the generator coordinates (θ_α , k , and d) and channel (β) is 200 (392) for the case of V2m-3R (G3RS2-3R) interaction. The total number of the Slater determinants superposed is 584 (1032) for the V2m-3R (G3RS2-3R) case. This is called full GCM calculation for ${}^8\text{Be}$.

D. $0s$, 1S , 3S , and 3D probabilities

In this study, we analyze the probabilities of the 1S , 3S , and 3D channels,

$$\mathcal{P}_{1S,3S,3D} = |\langle \Psi | \hat{P}_{1S,3S,3D} | \Psi \rangle|, \quad (34)$$

where $\hat{P}_{1S,3S,3D}$ are the projection operators onto the 1S , 3S , and 3D channels. We also calculate the “ $0s$ probability”

$$\mathcal{P}_{0s} = |\langle 0s | \Psi \rangle|^2, \quad (35)$$

where $|\Psi\rangle$ is the ground state wave function ($|\Psi_{4\text{He,g.s.}}\rangle$ for ${}^4\text{He}$ and $|\Psi_{8\text{Be,g.s.}}\rangle$ for ${}^8\text{Be}$), and $|0s\rangle$ is the state with the $(0s)^4$ configuration ($|\Phi_{4\text{He}}^{0s}\rangle$ for ${}^4\text{He}$ and $|\Phi_{2\alpha,0^+}^{0s}\rangle$ for ${}^8\text{Be}$). The probabilities of the correlated 1S and 3S components orthogonal to the $0s$ state is calculated as

$$\mathcal{P}_{1S,3S}^\perp = |\langle \Psi | \Lambda_{0s}^\perp \hat{P}_{1S,3S} \Lambda_{0s}^\perp | \Psi \rangle|^2, \quad (36)$$

$$\Lambda_{0s}^\perp \equiv 1 - |0s\rangle\langle 0s|. \quad (37)$$

Note that $\mathcal{P}_{1S,3S}^\perp$ somewhat depends on the adopted width parameter ν of the $0s$ orbit.

III. HAMILTONIAN AND INTERACTIONS

A. Hamiltonian

The Hamiltonian used in the present calculation is

$$\begin{aligned} \hat{H} &= \sum_i^A \hat{T}_i - \hat{T}_G \\ &+ \sum_{i<j}^A \left[\hat{V}_c(i, j) + \hat{V}_{\text{ls}}(i, j) + \hat{V}_t(i, j) + \hat{V}_{\text{Coulomb}}(i, j) \right], \end{aligned} \quad (38)$$

where \widehat{T}_i is the kinetic energy operator of i th nucleon. \widehat{T}_G is the total kinetic energy operator for the cm motion and its expectation value, $\langle \widehat{T}_G \rangle = 3\hbar\omega/4 (= 3\hbar^2\nu/2m)$, is constant in the present framework, where m is the mean value of proton and neutron masses.

The two-body interaction consists of the central (\widehat{V}_c), spin-orbit (\widehat{V}_{ls}), tensor (\widehat{V}_t), and Coulomb ($\widehat{V}_{\text{Coulomb}}$) parts. The Coulomb interaction for the protons is approximated by a seven-range Gaussian form.

Differently from our previous work [38], here we use a realistic interaction, Gaussian soft-core potential with three ranges (G3RS interaction) [43], which reproduces the NN -scattering phase shifts. The G3RS interaction consists of the central part with a soft core, spin-orbit part, and tensor part. The central part of G3RS has three-range Gaussian form as

$$\begin{aligned} \widehat{V}_c = & \widehat{P}_{ij}(^3E) \sum_{n=1}^3 V_{c,n}^{3E} \exp\left(-\frac{r_{ij}^2}{\eta_{c,n}^2}\right) \\ & + \widehat{P}_{ij}(^1E) \sum_{n=1}^3 V_{c,n}^{1E} \exp\left(-\frac{r_{ij}^2}{\eta_{c,n}^2}\right) \\ & + \widehat{P}_{ij}(^3O) \sum_{n=1}^3 V_{c,n}^{3O} \exp\left(-\frac{r_{ij}^2}{\eta_{c,n}^2}\right) \\ & + \widehat{P}_{ij}(^1O) \sum_{n=1}^3 V_{c,n}^{1O} \exp\left(-\frac{r_{ij}^2}{\eta_{c,n}^2}\right), \end{aligned} \quad (39)$$

where $\widehat{P}_{ij}(^1,^3E)$ and $\widehat{P}_{ij}(^1,^3O)$ are the projection operators to the $^1,^3E$ (singlet-even, triplet-even) and $^1,^3O$ (singlet-even, triplet-odd) states, respectively. We simply call the even (odd) part of the central interaction the central-even (central-odd) interaction.

The spin-orbit part of G3RS has a two-range Gaussian form as

$$\begin{aligned} \widehat{V}_{\text{ls}} = & \widehat{L}_{ij} \cdot \widehat{S}_{ij} \times \\ & \widehat{P}_{ij}(^3O) \sum_{n=1}^{n_{\text{max}}=3} V_{\text{ls},n}^{3O} \exp\left(-\frac{r_{ij}^2}{\eta_{\text{ls},n}^2}\right). \end{aligned} \quad (40)$$

For the tensor part, we use the version, where the G3RS tensor part is fitted with the r^2 -weighted Gaussian form (3-range fit tensor) given in the previous paper [38],

$$\begin{aligned} \widehat{V}_t = & r_{ij}^2 \widehat{S}_{ij} \times \\ & \left[\widehat{P}_{ij}(^3E) \sum_{n=1}^{n_{\text{max}}=3} V_{t,n}^{3E} \exp\left(-\frac{r_{ij}^2}{\eta_{t,n}^2}\right) \right. \\ & \left. + \widehat{P}_{ij}(^3O) \sum_{n=1}^{n_{\text{max}}=3} V_{t,n}^{3O} \exp\left(-\frac{r_{ij}^2}{\eta_{t,n}^2}\right) \right], \end{aligned} \quad (41)$$

$$r_{ij}^2 \widehat{S}_{ij} = 3(\widehat{\sigma}_i \cdot \widehat{r}_{ij})(\widehat{\sigma}_j \cdot \widehat{r}_{ij}) - (\widehat{\sigma}_i \cdot \widehat{\sigma}_j) r_{ij}^2, \quad (42)$$

where the standard tensor operator \widehat{S}_{ij} is dimensionless, and the range parameters $\eta_{t,n}$ is related to the width parameters β_n in the previous paper [38] as $\beta_n = 1/\eta_{t,n}^2$. The accuracy of the fitting is rather well within a few percent errors in energy for the ground state of ^4He .

B. Interaction parameters

We use ‘‘case 1’’ and ‘‘case 2’’ parameters of G3RS, which are labeled as G3RS1 and G3RS2. The central part of G3RS1 has the repulsive core of 2000 MeV height for the even-parity state, which is designed to reproduce the NN -scattering phase shift up to 600 MeV, whereas G3RS2 has the 500-630 MeV height and reproduces the NN -scattering up to 150 MeV. As mentioned before, the tensor part is approximated by the 3-range fit and therefore we note the case 1 and case 2 interactions as G3RS1-3R and G3RS2-3R, respectively. For comparison, we also use an effective interaction, ‘‘V2m-3R’’ introduced in the previous paper [38], which explicitly includes the tensor part but no repulsive core for the central part. Here the 3E part of the central interaction (Volkov No.2 [44]) is reduced to 60% of the original strength so as to reproduce the correct binding energy of ^4He after adding the tensor term within the AQCM-T model space. The spin-orbit part of V2m-3R is the same as G3RS1, and the tensor part is 3-range fit as in G3RS1-3R and G3RS2-3R. As shown in the next section, the binding energy and radius of ^4He are reasonably reproduced with G3RS2-3R and V2m-3R, but not satisfactory with G3RS1-3R within the present AQCM-T framework because of the high repulsive core. Therefore, we mainly use G3RS2-3R as the default interaction and compare the result with V2m-3R.

We also show results of conventional α -cluster model, where α clusters are expressed as pure $(0s)^4$ configurations without the NN correlation. Here effective interactions with no repulsive core for the central part and no tensor terms are used; the Volkov interaction with the same parameter as in the previous paper [38], labeled as ‘‘V2’’. Note that here only the central interaction gives non-zero contribution, and the spin-orbit and tensor contributions vanish even if the interaction contains such spin-dependent terms because the intrinsic spins are saturated in the $(0s)^4$ configuration. Even though V2 well describes basic properties of very light-mass nuclei, it is not sufficient for the saturation property of the nuclear matter; it causes the overbinding problem in heavier nuclei ($A \geq 16$). To avoid this problem, the odd-parity part has to be tuned for heavier nuclei by modifying the Majorana parameter as often done in conventional cluster model calculations. The Majorana parameter of V2 used here is adjusted to explain the α - α scattering phase shift.

We also show results obtained with the Brink-Boeker interaction, which does not have the tensor term but gives the nuclear saturation. We use ‘‘case four’’ of the Brink-Boeker interaction labeled as BB4 [45]. This interaction has a similar form to V2 (two range Gaussians)

but it has a quite shorter range for the odd part compared with V2 as $\eta_{c,2} = 0.4$ fm, which is almost a contact interaction. The BB4 interaction was designed to reproduce the energy and density of the nuclear matter at the saturation point as well as the binding energy of ${}^4\text{He}$, but instead, it cannot reproduce the NN and α - α scattering phase shifts. It also tends to give less binding energies for closed shell nuclei such as ${}^{16}\text{O}$ and ${}^{40}\text{Ca}$.

In Table I, we summarize the parameters of G3RS1-3R, G3RS2-3R, V2m-3R, V2, and BB4. It should be commented again that the same 3-range fit tensor is used in these three cases (G3RS1-3R, G3RS2-3R, and V2m-3R). The 1E part of V2m-3R is the same as that of V2, which is adjusted to reproduce the NN scattering length of the 1S channel. On the other hand, the 3E part of V2m-3R is reduced to 60% of that of V2 so as to reasonably describe the binding energy and radius of ${}^4\text{He}$ after including the tensor term. More details on the V2m-3R and V2 interactions are explained in our previous paper [38]. In Fig. 1, we show the r dependence for the central and tensor parts of G3RS1-3R, G3RS2-3R, and V2m-3R for the 3E channel. For the central part, the realistic interactions, G3RS1 (V_c :G3RS1) and G3RS2 (V_c :G3RS2), have the short-range repulsion and middle-range attraction. As clearly seen, G3RS1 has higher core and deeper pocket than G3RS2, whereas an effective interaction, the central part of V2m-3R (V_c :V2m), has no repulsive core and the attractive part has longer range. For the tensor part, here the original form of the G3RS2 interaction (V_t :G3RS2) and its 3-range fit (V_t :3R) are presented.

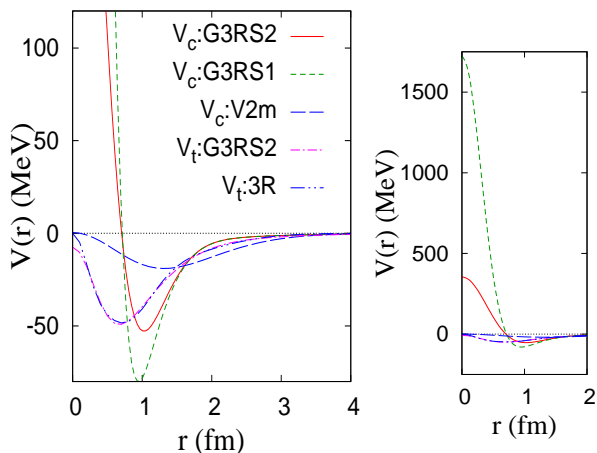


FIG. 1: (Color online) Left: radial (r) dependence of the 3E parts of the central (V_c) and tensor (V_t) interactions of G3RS1-3R, G3RS2-3R, and V2m-3R. The 3-range fit tensor is used in these three cases. Right: same as the left panel but on a different scale.

IV. APPLICATION TO ${}^4\text{He}$

We apply the AQCM-T method to ${}^4\text{He}$ using G3RS1-3R, G3RS2-3R, and V2m-3R. For comparison, we also show the results obtained with V2, where the model space is conventional cluster model with the $(0s)^4$ configuration, which we call the V2:0s calculation.

A. Results of ${}^4\text{He}$

The total energy (E), contributions of the kinetic term (T), central (V_c) and tensor (V_t) interactions, root-mean-square (rms) matter radius (R_m), and the probabilities of $0s$, 1S , 3S , and 3D channel of ${}^4\text{He}$ are listed in Table II. The results calculated with G3RS2-3R and V2m-3R reasonably reproduces the experimental binding energy and radius. For the energy contribution of each term (T , V_c , V_t), the two interactions, G3RS2-3R and V2m-3R, give similar results even though only the former has a short-range repulsion in the central part. They also give similar values for the D -state probability (\mathcal{P}_{3D}) meaning that the tensor contributions are qualitatively the same in both of them. On the other hand, for the S -wave, G3RS2-3R shows a significant mixing of the correlated 1S -state (\mathcal{P}_{1S}^\perp) and enhancement of the 3S correlations (\mathcal{P}_{3S}^\perp); the correlated 1S and 3S pairs beyond the $(0s)^4$ configuration are important owing to the short-range core of the central part. This result confirms that V2m-3R is an effective interaction, which explicitly includes the tensor interaction but the repulsive core in the central part is renormalized.

The results of G3RS1-3R are qualitatively similar to G3RS2-3R, but quantitatively different; the binding energy ($-E$) is underestimated compared with the experiment, whereas the size (R_m) is overestimated because of the higher repulsive core of G3RS1-3R (the height is 2000 MeV and 500 ~ 630 MeV in G3RS1 and G3RS2 in the central part, respectively).

These results indicate that the present AQCM-T method is applicable for a kind of *ab initio* calculation of ${}^4\text{He}$. Although the repulsive core of G3RS2 is lower than G3RS1, G3RS2 is still a “realistic force”, which reproduces the phase shift of low-energy NN scattering up to ~ 150 MeV. However, the present model space is not sufficient for G3RS1-3R, a realistic force with a significant height of the core capable of reproducing the NN scattering of higher energies.

Hereafter, we mainly focus on the results of G3RS2-3R and discuss features of the tensor and short-range correlations in ${}^4\text{He}$ and their roles in the two- α system, while comparing them with V2m-3R and V2:0s.

B. Contribution of each basis states in ${}^4\text{He}$

To clarify which channel (β) and momentum region (k) contribute to the tensor and short-range correlations

TABLE I: The parameter sets of G3RS1-3R, G3RS2-3R, V2m-3R, V2, and BB4 interactions. The range parameters of the tensor interaction, $\eta_{t,n}$, is related to the width parameters β_n in the previous paper [38] as $\beta_n = 1/\eta_{t,n}^2$, and $\beta_{1,2,3} = 0.53, 1.92, 8.95 \text{ fm}^{-2}$.

n	central			ls		tensor			
	1	2	3	1	2	1	2	3	
G3RS1-3R									
$\eta_{c/ls,n}$ (fm)	2.5	0.942	0.447	0.6	0.447	$\eta_{t,n}$ (fm)	1.3736	0.7217	0.3343
$V_{c/ls,n}^{3E}$ (MeV)	-5	-210	2000			$V_{t,n}^{3E}$ (MeV fm ⁻²)	-17.02	-209.89	-289.59
$V_{c/ls,n}^{1E}$ (MeV)	-5	-270	2000						
$V_{c/ls,n}^{3O}$ (MeV)	1.6667	-50	2500	-1050	600	$V_{t,n}^{3O}$ (MeV fm ⁻²)	5.27	62.91	89.87
$V_{c/ls,n}^{1O}$ (MeV)	10	50	2000						
G3RS2-3R									
$\eta_{c/ls,n}$ (fm)	2.5	0.942	0.6	0.6	0.4	$\eta_{t,n}$ (fm)	1.3736	0.7217	0.3343
$V_{c/ls,n}^{3E}$ (MeV)	-5	-210	500			$V_{t,n}^{3E}$ (MeV fm ⁻²)	-17.02	-209.89	-289.59
$V_{c/ls,n}^{1E}$ (MeV)	-5	-270	630						
$V_{c/ls,n}^{3O}$ (MeV)	1.6667	-50	400	-800	800	$V_{t,n}^{3O}$ (MeV fm ⁻²)	5.27	62.91	89.87
$V_{c/ls,n}^{1O}$ (MeV)	10	50	200						
V2m-3R									
$\eta_{c/ls,n}$ (fm)	1.8	1.01		0.6	0.447	$\eta_{t,n}$ (fm)	1.3736	0.7217	0.3343
$V_{c/ls,n}^{3E}$ (MeV)	-47.307	47.689				$V_{t,n}^{3E}$ (MeV fm ⁻²)	-17.02	-209.89	-289.59
$V_{c/ls,n}^{1E}$ (MeV)	-42.455	42.798							
$V_{c/ls,n}^{3O}$ (MeV)	12.13	-12.228		-1050	600	$V_{t,n}^{3O}$ (MeV fm ⁻²)	5.27	62.91	89.87
$V_{c/ls,n}^{1O}$ (MeV)	12.13	-12.228							
V2									
$\eta_{c,n}$ (fm)	1.8	1.01							
$V_{c,n}^{3E}$ (MeV)	-78.845	79.482							
$V_{c,n}^{1E}$ (MeV)	-42.455	42.798							
$V_{c,n}^{3O}$ (MeV)	12.13	-12.228							
$V_{c,n}^{1O}$ (MeV)	12.13	-12.228							
BB4									
$\eta_{c,n}$ (fm)	0.8	0.4							
$V_{c,n}^{3E}$ (MeV)	-1307.9	7228							
$V_{c,n}^{1E}$ (MeV)	-1307.9	7228							
$V_{c,n}^{3O}$ (MeV)	-60.4	7097.9							
$V_{c,n}^{1O}$ (MeV)	-60.4	7097.9							

in ^4He , we first analyze the squared overlap between the ground state wave function $\Psi_{4\text{He,g.s.}}$ and each basis state of AQCM-T. Each basis state is specified by the momentum parameter k and the channel β ; the squared overlap ($\mathcal{O}_\beta(k)$) for k in the $\beta = {}^3D$ channel is calculated as

$$\mathcal{O}_{3D}(k) = |\langle \Phi_{4\text{He},0^+}^{\text{AQCM-T}}(k, {}^3D) | \Psi_{4\text{He,g.s.}} \rangle|^2. \quad (43)$$

The squared overlaps for the $\beta = {}^{1,3}S$ channels are defined for their components orthogonal to $|0s\rangle$ as

$$\mathcal{O}_{1,3S}(k) = |\langle \Phi_{4\text{He},0^+}^{\text{AQCM-T}}(k, {}^{1,3}S) \Lambda_{0s}^\perp | \Psi_{4\text{He,g.s.}} \rangle|^2, \quad (44)$$

which measure the correlated ${}^{1,3}S$ components beyond the simple $0s$ (uncorrelated) state.

As shown in Fig. 2, in the two cases of G3RS2-3R (Fig. 2 (a)) and V2m-3R (Fig. 2 (c)), the 3D pair has

the largest overlap around $k \sim 2 \text{ fm}^{-1}$, indicating that this region of k dominantly contributes to the tensor correlation. This result is consistent with that of our previous paper [38] and also qualitatively in agreement with the discussion by Myo *et al.* [36], which pointed out the importance of the high-momentum tensor correlation. For the 3S and 1S channels, both of G3RS2-3R (Fig. 2 (a)) and V2m-3R (Fig. 2 (c)) contain the components in the lower momentum region of $k < 2 \text{ fm}^{-1}$, but one can see a striking difference in the high momentum regions; G3RS2-3R contains high momentum components of $k = 3 \sim 4 \text{ fm}^{-1}$ because of the short-range correlation caused by the repulsive core of the central interaction, but V2m-3R does not.

Let us turn to G3RS1-3R (Fig. 2 (b)). The 3D pair has the largest overlap around $k \sim 2 \text{ fm}^{-1}$, consistently with

TABLE II: Energies, radii (R_m), and probabilities (\mathcal{P}) of ^4He obtained by AQCM-T full configurations. For energies, the expectation values of the total energy (E), kinetic energy (T), central interaction (V_c), and tensor interaction (V_t) are shown. The calculated results for V2m-3R, G3RS2-3R, and G3RS1-3R are listed. The result of V2 with the $(0s)^4$ configuration is also shown (V2:0s). The experimental values of the total energy and radius are $E = -28.296$ MeV and $R_m = 1.455$ fm [46].

	V2m-3R	G3RS2-3R	G3RS1-3R	V2:0s
E (MeV)	-30.3	-26.5	-16.2	-27.9
T (MeV)	64.6	72.3	70.9	46.7
V_c (MeV)	-56.7	-58.4	-54.6	-75.3
V_t (MeV)	-39.9	-41.7	-33.9	
R_m (fm)	1.46	1.43	1.53	1.50
\mathcal{P}_{0s}	0.901	0.881	0.897	
$\mathcal{P}_{^3D}$	0.077	0.082	0.063	
$\mathcal{P}_{^3S}^\perp$	0.018	0.028	0.022	
$\mathcal{P}_{^1S}^\perp$	0.004	0.015	0.020	

G3RS2-3R and V2m-3R. It also contains high momentum components of the 3S and 1S channels in the $k = 3 \sim 4$ fm $^{-1}$ region caused by the short-range core, which are even enhanced compared with G3RS2-3R.

C. Truncation of the model space for ^4He

Next, we perform the AQCM-T calculation with truncated model space, where the configurations are reduced from the full calculation. In Fig. 3, we show the results of three-channel calculation with truncated configurations for k as $k \leq k_{\text{max}}$ (labeled by $3_{\text{ch}}^{k \leq k_{\text{max}}}$). The total energy (E), the contribution of each term of the Hamiltonian (T , V_c , V_t), and rms radius (R_m) are shown for G3RS2-3R (upper panel), G3RS1-3R (middle panel), and V2m-3R (lower panel). In V2m-3R (lower panel), the contribution of the central term (V_c) is almost unchanged in spite of the reduction of the k values and it stays at the value close to the one for the $(0s)^4$ configuration. The kinetic energy (T) gradually increases with increasing k_{max} in the range of $k_{\text{max}} \lesssim 3$ fm $^{-1}$, whereas the tensor interaction (V_t) compensates or even overcomes it. As a result, the total energy (E) gradually decreases and almost converges around $k_{\text{max}} \gtrsim 3$ fm $^{-1}$. This compensation of increasing kinetic energy and attractive tensor energy is the typical feature when the 3D component mixes, which can be also seen in G3RS1-3R (Fig. 3 (b)) and G3RS2-3R (Fig. 3 (a)). In G3RS2-3R (Fig. 3 (a)), the k_{max} dependence of the tensor (V_t) and total (E) energies are qualitatively similar to those of V2m-3R (Fig. 3 (c)); however, a clear difference is found in the central part (V_c), which gradually decreases in the 1 fm $^{-1} \lesssim k_{\text{max}} \lesssim 4$ fm $^{-1}$ region. Another difference is a rather rapid increase of

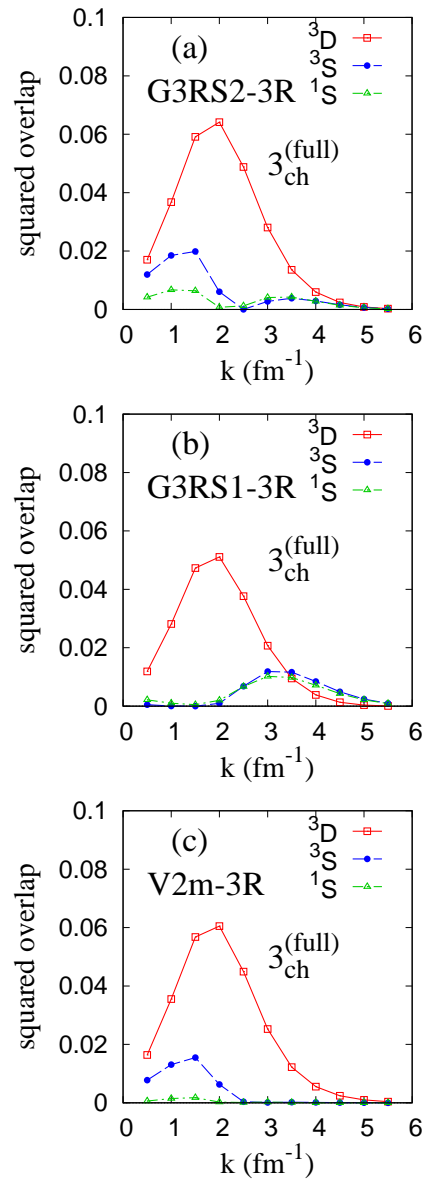


FIG. 2: (Color online) Squared overlaps $\mathcal{O}_\beta(k)$ for the $\beta = ^1S$, 3S , and 3D channels of ^4He (g.s.) obtained with the full configurations ($3_{\text{ch}}^{(\text{full})}$). The results for (a) G3RS2-3R, (b) G3RS1-3R, and (c) V2m-3R are shown.

the kinetic energy (T) seen in G3RS2-3R compared with V2m-3R. These behaviors of G3RS2-3R are qualitatively similar to G3RS1-3R, but quantitatively, the k_{max} dependence of the total, kinetic and central energies is stronger in G3RS1-3R. From these analyses, we can conclude that $k \lesssim 3$ fm $^{-1}$ is essential for the tensor correlation, while $k \lesssim 4$ fm $^{-1}$ contributes to the short-range correlation.

We perform further analysis based on the truncation of channels $\beta = \{^1S, ^3S, ^3D\}$; the two-channel calculation with $\beta = \{^3S, ^3D\}$ and the single-channel calculation only with $\beta = \{^3D\}$ are performed, while k values

TABLE III: Energies, radii (R_m), and probabilities (\mathcal{P}) of ${}^4\text{He}$ obtained with AQCM-T are compared with the $(0s)^4$ configuration. For energies, the expectation values of the total energy (E), kinetic energy (T), central interaction (V_c), and tensor interaction (V_t) are shown. The results of $3_{\text{ch}}^{(\text{full})}$, $2_{\text{ch}}^{(\text{full})}$, and $1_{\text{ch}}^{(\text{full})}$ calculations with full k values ($k = \{0.5, 1.0, \dots, 5.5\} \text{ fm}^{-1}$) for G3RS2-3R and V2m-3R are listed. The results of $3_{\text{ch}}^{(4)}$ (three channels with four k values, $k = \{1.5, 2.5, 3.5, 4.5\} \text{ fm}^{-1}$), $3_{\text{ch}}^{(3)}$ (three channels with three k values, $k = \{1.5, 2.5, 4.0\} \text{ fm}^{-1}$), $2_{\text{ch}}^{(3)}$ (two channels with three k values, $k = \{1.0, 2.0, 3.0\} \text{ fm}^{-1}$) are also shown. For the results of G3RS2-3R, the expectation values of the long-range ($V_{c,1}:\eta_{c,1} = 2.5 \text{ fm}$), middle-range ($V_{c,2}:\eta_{c,2} = 0.942 \text{ fm}$), and short-range ($V_{c,3}:\eta_{c,3} = 0.6 \text{ fm}$) terms of the central interactions are also shown.

G3RS2-3R							
β	$3_{\text{ch}}^{(\text{full})}$ { ${}^1S, {}^3S, {}^3D$ }	$2_{\text{ch}}^{(\text{full})}$ { ${}^3S, {}^3D$ }	$1_{\text{ch}}^{(\text{full})}$ { 3D }	$(0s)^4$	$3_{\text{ch}}^{(4)}$ { ${}^1S, {}^3S, {}^3D$ }	$3_{\text{ch}}^{(3)}$ { ${}^1S, {}^3S, {}^3D$ }	
k	full	full	full		{1.5, 2.5, 3.5, 4.5}	{1.5, 2.5, 4.0}	
E (MeV)	-26.5	-22.7	-18.5	2.2	-26.0	-25.1	
T (MeV)	72.3	68.9	59.8	46.7	73.6	72.9	
V_c (MeV)	-58.4	-51.2	-43.6	-45.3	-59.1	-58.4	
V_t (MeV)	-41.7	-41.9	-36.2		-41.8	-41.0	
$V_{c,1}$ (MeV)	-14.6	-14.3	-13.6	-14.3	-14.8	-14.7	
$V_{c,2}$ (MeV)	-124.1	-123.3	-108.7	-111.4	-125.5	-124.5	
$V_{c,3}$ (MeV)	80.3	86.5	78.7	80.4	81.2	80.8	
R_m (fm)	1.43	1.44	1.49	1.50	1.41	1.41	
\mathcal{P}_{0s}	0.881	0.891	0.919	1.000	0.885	0.886	
\mathcal{P}_{3D}	0.082	0.085	0.081		0.081	0.080	
\mathcal{P}_{3S}^\perp	0.028	0.024			0.027	0.026	
\mathcal{P}_{1S}^\perp	0.015				0.015	0.015	
V2m-3R							
β	$3_{\text{ch}}^{(\text{full})}$ { ${}^1S, {}^3S, {}^3D$ }	$2_{\text{ch}}^{(\text{full})}$ { ${}^3S, {}^3D$ }	$1_{\text{ch}}^{(\text{full})}$ { 3D }	$(0s)^4$	$2_{\text{ch}}^{(3)}$ { ${}^3S, {}^3D$ }		
k	full	full	full		{1.0, 2.0, 3.0}		
E (MeV)	-30.3	-30.0	-28.2	-8.3	-28.2		
T (MeV)	64.6	65.7	58.9	46.7	64.8		
V_c (MeV)	-56.7	-57.1	-53.7	-55.8	-57.4		
V_t (MeV)	-39.9	-40.2	-35.0		-37.3		
R_m (fm)	1.46	1.44	1.49	1.50	1.43		
\mathcal{P}_{0s}	0.901	0.903	0.927	1.00	0.905		
\mathcal{P}_{3D}	0.077	0.078	0.073		0.080		
\mathcal{P}_{3S}^\perp	0.018	0.019			0.016		
\mathcal{P}_{1S}^\perp	0.004						

are not truncated. They are labeled as $3_{\text{ch}}^{(\text{full})}$, $2_{\text{ch}}^{(\text{full})}$, and $1_{\text{ch}}^{(\text{full})}$, respectively. In Table III, the contribution of each term of the Hamiltonian, radius, and probabilities in the three cases ($3_{\text{ch}}^{(\text{full})}$, $2_{\text{ch}}^{(\text{full})}$, and $1_{\text{ch}}^{(\text{full})}$) for G3RS2-3R and V2m-3R are shown together with those for the $(0s)^4$ configuration. In the case of G3RS2-3R, the only inclusion of the 3D channel ($1_{\text{ch}}^{(\text{full})}$) describes major part of the tensor correlation. However, as seen in the significant difference between $1_{\text{ch}}^{(\text{full})}$ and $2_{\text{ch}}^{(\text{full})}$, the mixing of the correlated 3S component also somewhat contributes to the energy gains of the central (V_c) and tensor (V_t) terms (the difference is -5.7 MeV for V_t and -7.6 MeV for V_c). The 1S channel, which is included in $3_{\text{ch}}^{(\text{full})}$, provides further decrease of

the total energy (E) through the central interaction; the decrease of E is 3.8 MeV . In contrast, in V2m-3R, the inclusion of 1S in $3_{\text{ch}}^{(\text{full})}$ gives almost no effect.

For the purpose of applying AQCM-T to heavier systems such as ${}^8\text{Be}$, it is desirable to reduce the number of basis wave functions in order to save the computational cost. For this aim, we select limited numbers of the configurations, which can efficiently describe the essential properties of ${}^4\text{He}$. For G3RS2-3R, we choose four values of k , $k = \{1.5, 2.5, 3.5, 4.5\} \text{ (fm}^{-1}\text{)}$ in the three channel calculation, which is labeled as $3_{\text{ch}}^{(4)}$. As shown in Table III, $3_{\text{ch}}^{(4)}$ describes basic properties of ${}^4\text{He}$ with almost equal quality to the full calculation, $3_{\text{ch}}^{(\text{full})}$.

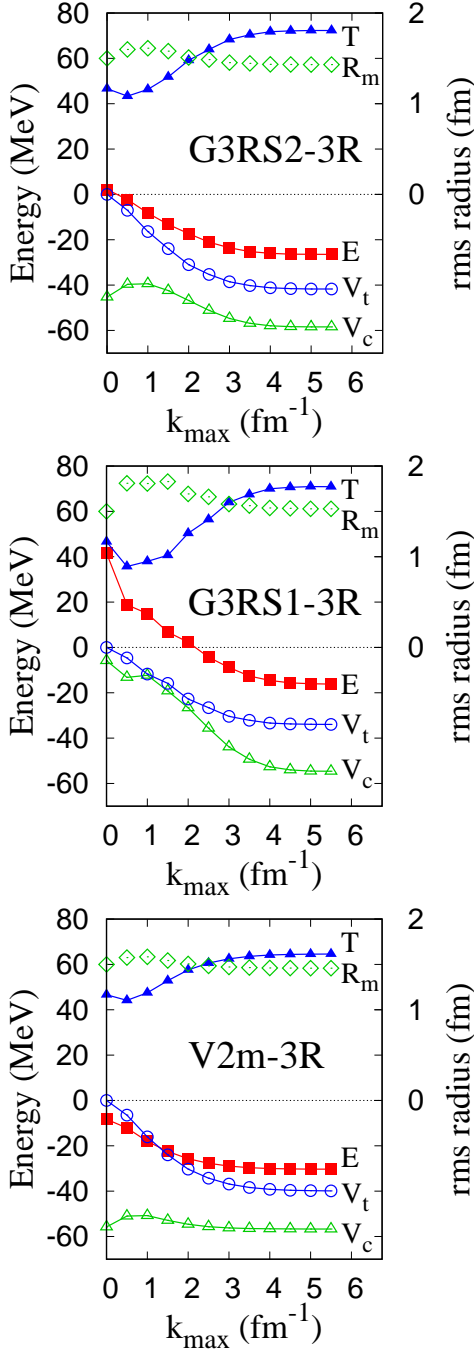


FIG. 3: (Color online) Energies (left vertical axis) and radii (right vertical axis) of ${}^4\text{He}$ for the 3-channel calculation ($3_{\text{ch}}^{k \leq k_{\text{max}}}$) with the truncation for the momentum k ($k \leq k_{\text{max}}$). For energies, the expectation values of the total energy (E), kinetic energy (T), central interaction (V_c), and tensor interaction (V_t) are shown. The radii (R_m) are shown by disconnected diamonds. The upper-, middle-, and lower panels show the results of G3RS2-3R, G3RS1-3R, and V2m-3R, respectively.

We also searched for even smaller set and found that $k = \{1.5, 2.5, 4.0\}$ (fm^{-1}) and three channels give reasonable result, labelled as $3_{\text{ch}}^{(3)}$. For V2m-3R, we adopt the same set as in the previous paper [38]; 2-channel with three k values, $k = \{1.0, 2.0, 3.0\}$ (fm^{-1}), labeled as $2_{\text{ch}}^{(3)}$, also gives reasonably agreement with the full calculation.

D. NN pair wave functions in ${}^4\text{He}$

Using the partial wave expansion of $\varphi_k^+(\mathbf{r})$ shown in Eq. (10), we reconstruct the wave function of the correlated NN pair called pair wave function, noted as $\phi_{NN}(r)$. Here, the pair wave functions $\phi_{NN}(r)$ are the correlated NN pairs in the 1S , 3S , and 3D channels,

$${}^1S: \quad \phi_g(\mathbf{r}_g)\phi_g(\mathbf{r}'_g) \otimes \phi_{NN}^{1S}(r)\varphi_0^{(0)}(r') \otimes Y_{00}Y_{00} \otimes \chi_0^\sigma\chi_0^\sigma \otimes [\chi_1^\tau\chi_1^\tau]_{T=0},$$

$${}^3S: \quad \phi_g(\mathbf{r}_g)\phi_g(\mathbf{r}'_g) \otimes \phi_{NN}^{3S}(r)\varphi_0^{(0)}(r') \otimes Y_{00}Y_{00} \otimes [\chi_1^\sigma\chi_1^\sigma]_{s=0} \otimes \chi_0^\tau\chi_0^\tau,$$

and

$${}^3D: \quad \phi_g(\mathbf{r}_g)\phi_g(\mathbf{r}'_g) \otimes \phi_{NN}^{3D}(r)\varphi_0^{(0)}(r') \otimes [Y_{20}Y_{00} \otimes [\chi_1^\tau\chi_1^\tau]_{s=2}]_{J=0} \otimes \chi_0^\sigma\chi_0^\sigma,$$

respectively.

The pair wave functions in ${}^4\text{He}$ are shown in Fig. 4. The radial (r) dependence of the 3E parts of the central (V_c) and tensor (V_t) interactions are also shown to see the correspondence.

Figure 4 (a) shows the pair wave functions of the full calculation ($3_{\text{ch}}^{(\text{full})}$) obtained with G3RS2-3R. Here $\phi_{NN}^{3D}(r)$ (line “ 3D ”) shows a peak in the middle-range region, $r \sim 1$ fm. Also, $\phi_{NN}^{3S}(r)$ and $\phi_{NN}^{1S}(r)$ (lines “ 3S ” and “ 1S ”) are peaked in the middle-range ($r \sim 1$ fm) region corresponding to the pocket of the central-even interaction, but they are strongly suppressed in the $r < 1$ fm region because of the short-range repulsion. In the middle-range region, the amplitude of $\phi_{NN}^{3S}(r)$ is larger than $\phi_{NN}^{1S}(r)$ because of the additional attraction caused by the tensor interaction incorporated through the 3S - 3D coupling. Since this additional attraction is particularly strong at the peak position of $\phi_{NN}^{3D}(r)$, it enhances the amplitude of $\phi_{NN}^{3S}(r)$ in this $r \sim 1$ fm region and efficiently contributes to the energy gain of the central-even interaction. This appearance of distinct peaks in the 1S and 3S channels is a unique feature of the realistic interactions, G3RS2-3R (Fig. 4 (a)) and G3RS1-3R (Fig. 4 (d)), but cannot be seen in the case of effective interactions without the short-range core of the central interaction as in V2m-3R (Fig. 4 (f)).

Figure 4 (b) is also for G3RS2-3R, but this shows the result of $3_{\text{ch}}^{k \leq k_{\text{max}}}$ with different k_{max} values. As

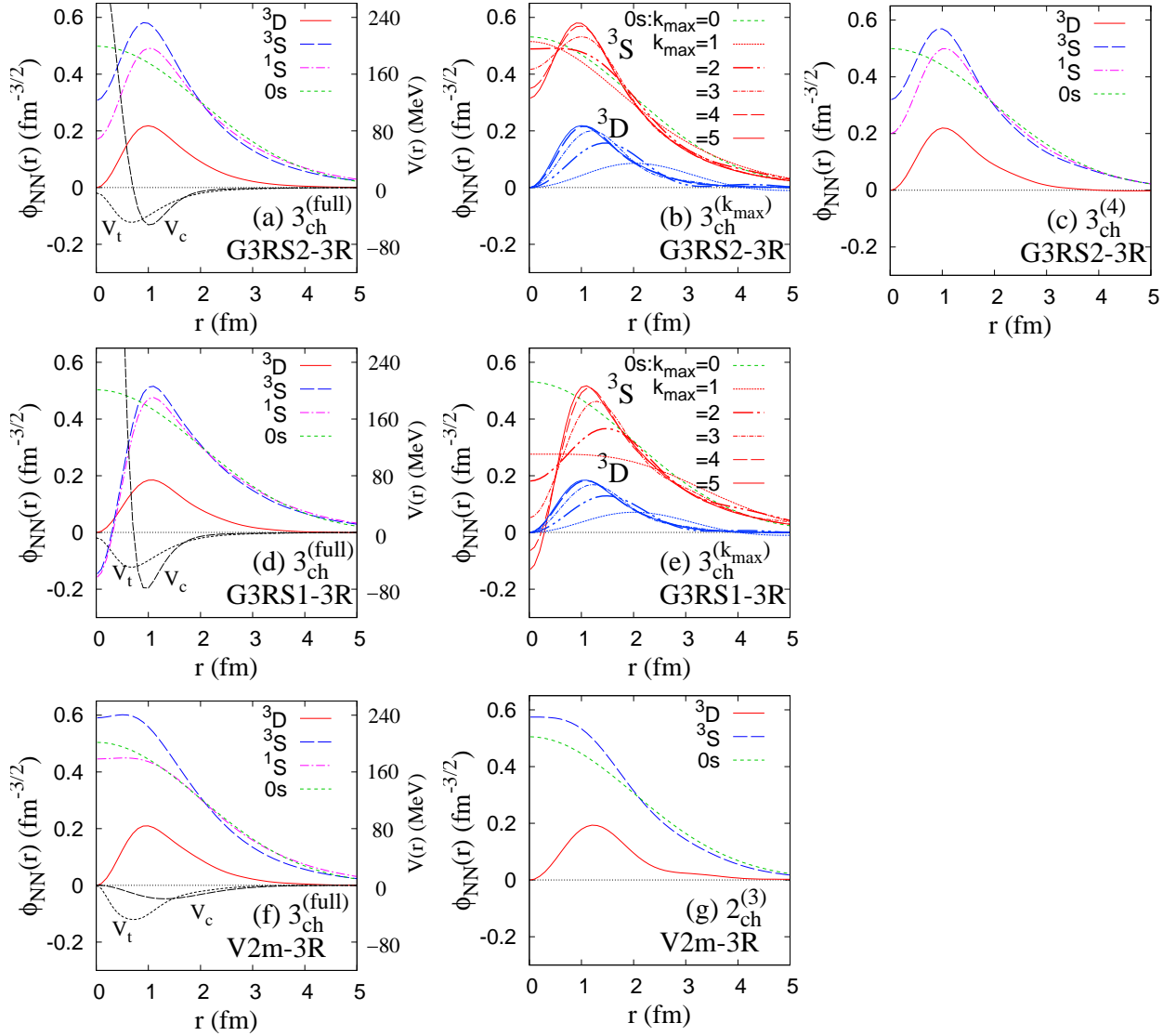


FIG. 4: (Color online) Pair wave functions $\phi_{NN}(r)$ of $^4\text{He}(\text{g.s.})$ for the 3D , 3S , and 1S channels and $0s$ component obtained with the full configurations and various interactions, G3RS2-3R (a), G3RS1-3R (d), and V2m-3R (f). The radial dependence of the 3E parts of the central (V_c) and tensor (V_t) interactions are shown in the right vertical axis. Those of 3-channel calculation with truncated k , $k \leq k_{\text{max}}$ obtained with G3RS2-3R (b) and G3RS1-3R (e). (c): $3_{\text{ch}}^{(4)}$, 3-channel calculation with $k = \{1.5, 2.5, 3.5, 4.5\} \text{ fm}^{-1}$, obtained with G3RS2-3R, and (g): $2_{\text{ch}}^{(3)}$, 2-channel calculation with $k = \{1.0, 2.0, 3.0\} \text{ fm}^{-1}$, obtained with V2m-3R. The pair wave functions of $(0s)^4$ corresponding to $k_{\text{max}} = 0$ are shown in (b) and (e).

k_{max} increases, the amplitude of $\phi_{NN}^{3D}(r)$ (lines “ 3D ”) rapidly grows, where the configurations of $k \lesssim 3 \text{ fm}^{-1}$ largely contribute to the peak in the middle-range region ($r \sim 1 \text{ fm}$). For $\phi_{NN}^{3S}(r)$ (“ 3S ”), the middle-range part grows up and the short-range part is suppressed with increasing k_{max} . In particular, the high-momentum configurations with $k = 3 \sim 4 \text{ fm}^{-1}$ contribute to both the enhancement of the middle-range part and the suppression of the short-range part, whereas the configurations with lower momenta ($k \lesssim 2 \text{ fm}^{-1}$) mainly contribute to the reduction of the tail part in the long-range region

around $r \sim 3 \text{ fm}$ compared with the uncorrelated $0s$ state (line “ $0s: k_{\text{max}} = 0$ ”).

In Fig. 4 (c), the pair wave functions for G3RS2-3R obtained with reduced number of the basis states, $3_{\text{ch}}^{(4)}$, are shown, which reasonably reproduce the basic properties of the full 3-channel calculation, $3_{\text{ch}}^{(\text{full})}$.

Figures 4 (d) and (e) show the pair wave functions of G3RS1-3R, whereas (f) and (g) are for V2m-3R. For G3RS1-3R, $\phi_{NN}^{3S}(r)$ and $\phi_{NN}^{1S}(r)$ (lines “ 3S ” and “ 1S ” in Fig. 4 (d)) show further suppression of the amplitudes in the short range and enhancement of a narrower peak in

the middle range compared with G3RS2-3R (lines “ 3S ” and “ 1S ” in Fig. 4 (a)), because of higher repulsion (in short range) and deeper attraction (in the middle range) of the central-even interaction. For V2m-3R, the S -wave pair wave functions, $\phi_{NN}^3(r)$ and $\phi_{NN}^1(r)$ (lines “ 3S ” and “ 1S ” in Fig. 4 (f)), do not show such suppression in the short range nor remarkable peak in the middle range since V2m-3R has no repulsive core. Thus, S -wave pair wave functions, $\phi_{NN}^3(r)$ and $\phi_{NN}^1(r)$, show different features in the cases of G3RS2-3R and V2m-3R depending on the presence of the repulsive core of the central interaction, even though the contributions of the central interactions are similar in the calculated energy. On the other hand, the D -wave pair wave function ($\phi_{NN}^3(r)$) shows quite similar features in the three cases of G3RS2-3R, G3RS1-3R, and V2m-3R.

V. APPLICATION TO ^8Be

In this section, we investigate ^8Be with the present AQCM-T method. To reduce the calculation costs, the correlated α cluster of $3_{\text{ch}}^{(4)}$ is adopted for G3RS2-3R, whereas $2_{\text{ch}}^{(3)}$ is adopted for V2m-3R, which can reasonably describe basic properties of ^4He . These are fixed in all the results of ^8Be in this section. They are compared with V2:0s, the conventional two- α cluster calculation with the V2 interaction.

A. Fixed- d calculation of ^8Be

The energies and probabilities of 3D and $0s$ components obtained with the fixed- d and full GCM calculations are compared in Table IV. We also show the values for the ideal $^4\text{He}(\text{g.s.})$ - $^4\text{He}(\text{g.s.})$ state in the asymptotic region of $d_\alpha \rightarrow \infty$, which are evaluated as twice the ^4He energies calculated with the consistent model space. Note that a constant energy shift of $T_r = \langle \hat{T}_G \rangle / 3 = \hbar\omega/4$ is added to the kinetic and total energies for the ideal $^4\text{He}(\text{g.s.})$ - $^4\text{He}(\text{g.s.})$ state, which corresponds to the increase of the energy due to the localization of the inter-cluster motion by fixing d , even though d is quite large. The two- α threshold energy estimated from $^4\text{He}(\text{g.s.})$ is also shown.

As the distance d increases, each energy component gets closer to the values for the ideal $^4\text{He}(\text{g.s.})$ - $^4\text{He}(\text{g.s.})$ state, indicating that two ^4He come to their ground state. However, even at large d values, there still remain some differences compared with the values for the ideal $^4\text{He}(\text{g.s.})$ - $^4\text{He}(\text{g.s.})$ state; the total energy ($\langle E \rangle_{2\alpha}$) is higher by about 4 MeV, and the absolute values of kinetic ($\langle T \rangle_{2\alpha}$) and tensor ($\langle V_t \rangle_{2\alpha}$) energies are smaller by about 10 MeV. Also, the $0s$ probability (\mathcal{P}_{0s}) is smaller by about 5%. These differences may originate from the limitation of the present AQCM-T framework for ^8Be ; the second-order correlation effect that both of two α

clusters are simultaneously correlated, is omitted. From the energy at $d_{\text{max}} (= 8 \text{ fm})$, this defect of the binding energy due to the missing second-order correlation is estimated to be 5.4 MeV and 3.1 MeV in G3RS2-3R and V2m-3R, respectively. This artifact should be taken into account in the following discussion.

As two α clusters approach, the total energy increases because of the increase of the kinetic energy and decrease of the attractive effect of the potential energy. In particular, the reduction of the tensor attraction significantly contributes in the $d \leq 2 \text{ fm}$ region, in which the D -state probability is strongly suppressed. In Figs. 5 and 6, the energy and probability of each channel are plotted as functions of d . The former is for the absolute energies, whereas the latter is for the relative energies measured from $d_{\text{max}} (= 8 \text{ fm})$. The \mathcal{P}_{3D} probability and that for the correlated S -wave pair orthogonal to the uncorrelated $(0s)^4$ state for each α ($1 - \mathcal{P}_{0s} - \mathcal{P}_D$) are also plotted. In the case of V2:0s (open circle in Fig. 5), the total energy (E) somewhat increases when two α clusters get closer mainly because of the increases in the kinetic (T) energy and central-odd interaction ($V_{c,\text{odd}}$). The former is the Pauli blocking effect between α clusters; four nucleons in one of the α clusters are raised up to the $0p$ -orbits from the $0s$ -orbits, which contributes in the $d \leq 3 \text{ fm}$ region. The latter is responsible for the repulsion in the $d \leq 4 \text{ fm}$ region ($d \leq 3 \text{ fm}$ in the BB4:0s (open triangle) case). These two repulsions are long-distance effects, which are rather general features of the α - α potential and seen both in G3RS2-3R (solid square) and V2m-3R (solid triangle). It should be commented that the effect coming from the central-odd part in G3RS2-3R is smaller by a factor of 2/3 than in V2m-3R and V2:0s.

However, in the G3RS2-3R (solid square in Fig. 5) and V2m-3R (solid triangle) cases, another repulsive effect at short distances comes from the tensor suppression. In the long-distance region ($d \sim 8 \text{ fm}$), the tensor interaction (V_t) significantly contributes to the binding energy of each α cluster through the mixing of the 3D state. Although the 3D -state mixing induces some increase of the kinetic energy (T), this is compensated by the larger gain of the attractive tensor contribution. As α clusters come close to each other, this tensor contribution is reduced, and the 3D state (\mathcal{P}_D in Fig. 6) is suppressed because of the Pauli blocking of nucleons in two α clusters. These effects work in the region of $d \leq 2 \text{ fm}$, relatively shorter distance region compared with the repulsive effects of the kinetic and central-odd parts in the longer distance region. Note that weakening of the kinetic energy in this region is also a signal of the tensor suppression. Comparing the results of G3RS2-3R and V2m-3R, the repulsive effect at short d is slightly larger in G3RS2-3R than in V2m-3R; the energy is higher by about 15 MeV at $d = 1 \text{ fm}$. This is attributed to the additional effect of the central-even interaction (mainly 3E) caused by the reduction of the correlated S -wave pair, $1 - \mathcal{P}_{0s} - \mathcal{P}_D$, which can be seen in the $d \leq 2 \text{ fm}$ region in the case of G3RS2-3R (Fig. 6 (a)), but not in V2m-3R

TABLE IV: Each component of the Hamiltonian and the probabilities of the $0s$ and 3D components in ${}^8\text{Be}$ obtained with the fixed- d calculation for G3RS2-3R and V2m-3R. For energies, the expectation values of the total energy (E), kinetic energy (T), central interaction (V_c), and tensor interaction (V_t) are shown. The values for the ideal ${}^4\text{He}(\text{g.s.})$ - ${}^4\text{He}(\text{g.s.})$ state in the asymptotic region of $d_\alpha \rightarrow \infty$ and threshold (2α thres.) energies are evaluated as twice the ${}^4\text{He}$ energy obtained with a consistent model space. The constant shift of $T_r = \hbar\omega/4 = 5.2$ MeV is added to the kinetic and total energies for the ideal ${}^4\text{He}(\text{g.s.})$ - ${}^4\text{He}(\text{g.s.})$ state, corresponding to the localization of clusters with fixed relative distance. The values of the $0s$ state for the conventional two- α cluster model with the V2 interaction are also shown. All energies are in MeV.

G3RS2-3R						
d (fm)	$\langle E \rangle_{2\alpha}$	$\langle T \rangle_{2\alpha}$	$\langle V_c \rangle_{2\alpha}$	$\langle V_t \rangle_{2\alpha}$	\mathcal{P}_{0s}	\mathcal{P}_{3D}
1	24.8	153.1	-114.5	-17.8	0.95	0.04
2	-2.7	157.8	-121.0	-43.8	0.89	0.09
3	-29.2	153.8	-122.3	-65.0	0.85	0.11
4	-39.0	144.5	-117.6	-69.9	0.84	0.12
5	-40.5	140.1	-114.4	-69.9	0.84	0.12
6	-40.6	139.3	-113.6	-69.8	0.84	0.12
GCM	-45.8	138.2	-116.8	-70.9	0.83	0.12
2α thres.	-50.3					
	$2\langle E \rangle_\alpha + T_r$	$2\langle T \rangle_\alpha + T_r$	$2\langle V_c \rangle_\alpha$	$2\langle V_t \rangle_\alpha$	$\{\mathcal{P}_{0s}\}_\alpha^2$	
${}^4\text{He}(\text{g.s.})$ - ${}^4\text{He}(\text{g.s.})$	-45.1	151.0	-116.9	-82.1	0.78	
V2m-3R						
d (fm)	$\langle E \rangle_{2\alpha}$	$\langle T \rangle_{2\alpha}$	$\langle V_c \rangle_{2\alpha}$	$\langle V_t \rangle_{2\alpha}$	\mathcal{P}_{0s}	\mathcal{P}_{3D}
1	3.4	148.1	-132.8	-16.1	0.94	0.04
2	-18.6	149.1	-132.3	-40.0	0.90	0.09
3	-39.7	142.3	-127.0	-59.8	0.86	0.12
4	-47.4	132.3	-119.7	-64.4	0.86	0.12
5	-47.8	127.6	-115.3	-64.2	0.86	0.12
6	-47.4	126.7	-113.9	-64.1	0.86	0.12
GCM	-51.3	124.2	-115.4	-64.2	0.82	0.12
2α thres.	-56.4					
	$2\langle E \rangle_\alpha + T_r$	$2\langle T \rangle_\alpha + T_r$	$2\langle V_c \rangle_\alpha$	$2\langle V_t \rangle_\alpha$	$\{\mathcal{P}_{0s}\}_\alpha^2$	
${}^4\text{He}(\text{g.s.})$ - ${}^4\text{He}(\text{g.s.})$	-51.2	134.9	-114.9	-74.5	0.78	
V2:0s						
d (fm)	$\langle E \rangle_{2\alpha}$	$\langle T \rangle_{2\alpha}$	$\langle V_c \rangle_{2\alpha}$	$\langle V_t \rangle_{2\alpha}$	\mathcal{P}_{0s}	\mathcal{P}_{3D}
1	-38.5	145.3	-187.6	0	1	0
2	-45.7	132.1	-181.4	0	1	0
3	-51.8	116.0	-171.1	0	1	0
4	-53.0	104.1	-160.2	0	1	0
5	-51.3	99.5	-153.5	0	1	0
6	-50.2	98.6	-151.3	0	1	0
GCM	-55.5	100.7	-159.2	0		0
2α thres.	-55.8					
	$2\langle E \rangle_\alpha + T_r$	$2\langle T \rangle_\alpha + T_r$	$2\langle V_c \rangle_\alpha$	$2\langle V_t \rangle_\alpha$	$\{\mathcal{P}_{0s}\}_\alpha^2$	
${}^4\text{He}(\text{g.s.})$ - ${}^4\text{He}(\text{g.s.})$	-50.6	98.5	-150.7	0	1 0	

(Fig. 6 (b)). These repulsive effects at short distances related to the tensor (V_t in Fig. 5) and central-even interactions ($V_{c,\text{even}}$) are attributed to the high-momentum correlations of nucleons in the α clusters. More detailed discussions are given later in subsection V C.

B. Full GCM calculation for ${}^8\text{Be}$

We perform full GCM calculation by superposing the wave functions with different values for the generator coordinate d ($d = 1, \dots, 8$ fm). The calculated energy and probability for G3RS2-3R, V2m-3R, and V2:0s are shown

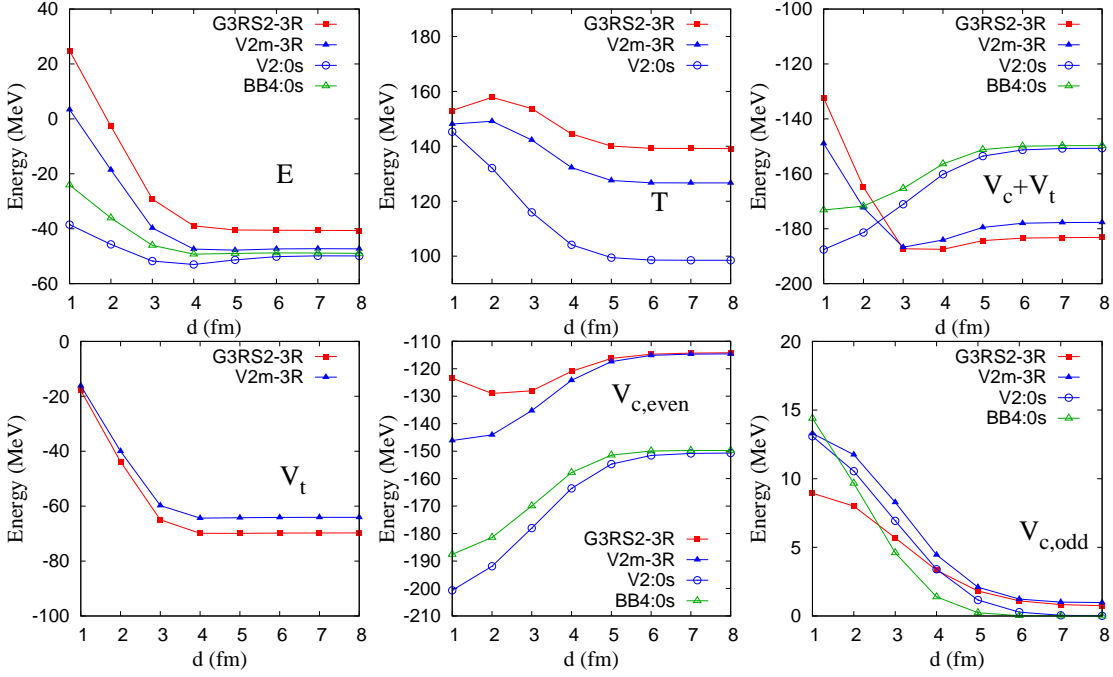


FIG. 5: (Color online) Each component of the Hamiltonian for ${}^8\text{Be}$ obtained with full configurations ($3_{\text{ch}}^{\text{full}}$) but fixed d . The results of G3RS2-3R and V2m-3R are compared, and the values of the $0s$ state for the V2 (V2:0s) and BB4 (BB4:0s) interactions are also shown. The expectation values of the total energy (E), kinetic energy (T), sum of central and tensor interactions ($V_c + V_t$) are shown in the top-left, top-middle, and top-right panels, and those of the tensor (V_t), central-even ($V_{c,\text{even}}$), and central-odd ($V_{c,\text{odd}}$) components are shown in the bottom-left, bottom-middle, and bottom-right panels, respectively.

in the row “GCM” of Table IV. Compared with the minimum energy of the fixed- d calculation, the total energy is lower by about 5 MeV because the kinetic energy coming from the localization of the inter-cluster motion is released by the superposition of different d configurations in the GCM calculation. The relative energy E_r of ${}^8\text{Be}(0^+)$ measured from the two- α threshold is 7.8 MeV, 5.0 MeV, and 0.3 MeV for G3RS2-3R, V2m-3R, and V2:0s, respectively. The experimental value of $E_r = 0.1$ MeV is well reproduced with V2:0s, but not with G3RS2-3R and V2m-3R. This shortcoming dominantly comes from the missing second-order correlation in the asymptotic region. As mentioned previously, this effect is 5.4 MeV (3.1 MeV) for G3RS2-3R (V2m-3R). However, even with this effect, the energy is still higher by a few MeV, implying that some attractive effect is still missing. We do not know its reason, but three-body interactions might help for the additional attraction.

The solid squares in Fig. 7 (a) and (c) show the squared overlap between the full GCM solution and the $0s$ state, $|\langle \Phi_{2\alpha,0^+}^{0s}(d) | \Psi_{2\alpha,0^+}^{\text{GCM}} \rangle|^2$, for G3RS2-3R and V2m-3R, respectively, which are normalized to the $0s$ probability (\mathcal{P}_{0s}) obtained at $d_{\text{max}} = 8$ fm. The total energies of the fixed- d calculation are shown as solid squares in Fig. 7 (b) and (d) for G3RS2-3R and V2m-3R, respectively, which show the relative energies measured from the value at $d_{\text{max}} = 8$ fm. Here the energies of the full GCM results

are also shown as the horizontal lines. Compared with V2:0s, both amplitudes of G3RS2-3R and V2m-3R are pushed out because of the less two- α binding.

In order to remove this artifact coming from the less binding, we tune the odd part of the central interaction of G3RS2-3R and V2m-3R so that the GCM calculations give the same two- α bindings as the V2:0s calculation. In Fig. 7, we adjust the relative energies measured from $d_{\text{max}} (= 8$ fm) obtained with the fixed- d calculations. For V2m-3R, we reduce the odd part of the central interaction to 10% of the original strength (V2m $_{0.1\text{odd}}$ -3R) and compare with V2:0s with the default Majorana parameter of $m = 0.60$ (V2 $_{0.60}$:0s). For G3RS2-3R, we remove the odd part of the central interaction (G3RS $_{w/o}$ odd) and compare with V2:0s with $m = 0.66$ (V2 $_{0.66}$:0s), corresponding to the enhancement of the central-odd interaction by 80%. The $0s$ normalized overlap for G3RS2-3R (Fig. 7 (a) solid square) and V2m-3R (Fig. 7 (c) solid square) show similar d -dependence of to that of the V2:0s results (solid triangle), which is a little bit surprising because the α - α energy curves of G3RS2-3R (Fig. 7 (b) solid square) and V2m-3R (Fig. 7 (d) solid square) show the repulsion at short distances compared with V2:0s (solid triangle).

It should be commented that the normalized $0s$ overlap introduced here is a good measure of the two- α structure at d . However, this quantity may contain not only the

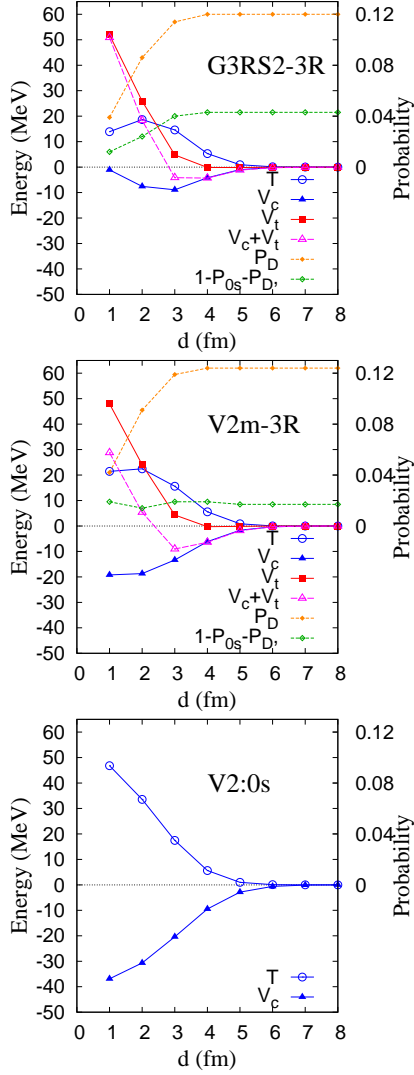


FIG. 6: (Color online) Each component of the Hamiltonian (left vertical axis) and D state probability (right vertical axis) of ${}^8\text{Be}$ obtained with the full configurations ($3_{\text{ch}}^{\text{full}}$) of AQCM-T but with fixed d . In each panel, the expectation values of the kinetic energy (T), the central (V_c) and the tensor (V_t) interactions, and sum of central and tensor interactions ($V_c + V_t$) are shown. Relative energies are measured from the values at d_{max} ($= 8$ fm) are plotted as functions of d . The results for G3RS2-3R, V2m-3R, and V2:0s are shown in the top, middle, and bottom panels, respectively. Right vertical axis: The probability of the 3D component (\mathcal{P}_{3D}) and that of the correlated S -wave component ($1 - \mathcal{P}_{0s} - \mathcal{P}_{3D}$).

unpolarized two- α component but also the polarized component. To extract only the unpolarized α component, we calculate the squared overlap between $\Psi_{2\alpha,0^+}^{\text{GCM}}$ and the frozen- α wave function $\Psi_{2\alpha,0^+}^{\text{frozen}}(d)$ defined in Eq. (27). The result is shown as cross symbols in Fig. 7 (a) and (c). In the $d \geq 3$ fm region, there is no difference, because the core polarization is small in this region. At

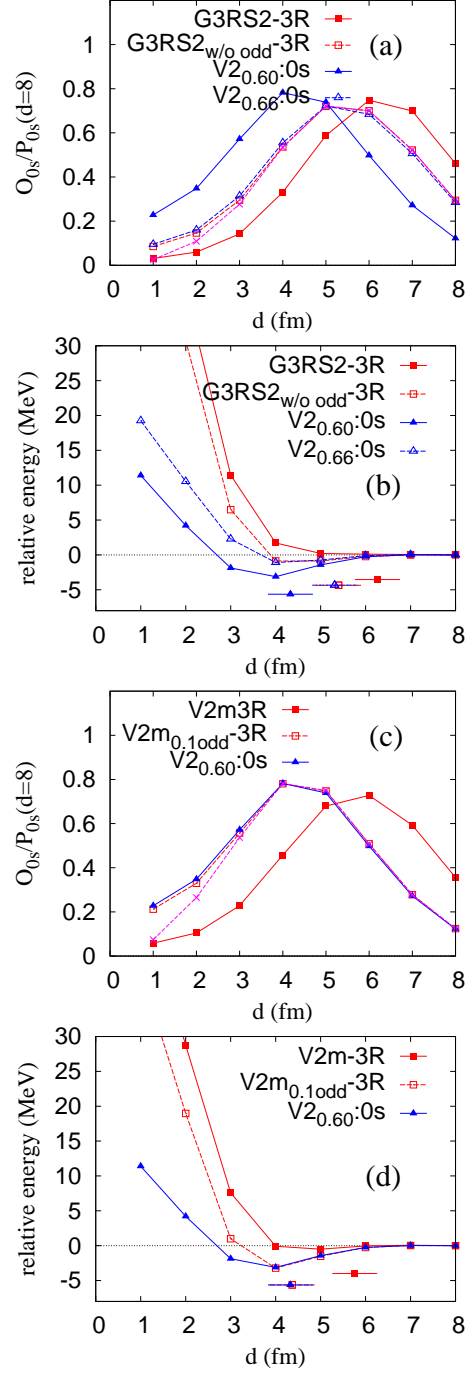


FIG. 7: (Color online) Squared overlap at d between the full GCM calculation of AQCM-T and the $0s$ state of ${}^8\text{Be}$. (a): G3RS2-3R and that without the odd part of the central interaction (G3RS_{w/o odd}) are compared with V2:0s with the Majorana parameter of $m = 0.60$ (V2_{0.60}:0s) and 0.66 (V2_{0.66}:0s). (c): V2m-3R with the default value for the central-odd part and weakened one with a factor of 0.1 (V2m_{0.1odd}-3R) are compared with V2:0s with $m = 0.60$ (V2_{0.60}:0s). The squared overlap is scaled by $1/\mathcal{P}_{0s}$ with the value of \mathcal{P}_{0s} at d_{max} ($= 8$ fm). Squared overlap with the frozen- α wave function is also shown as cross symbols in (a) and (c). Relative energy measured from d_{max} ($= 8$ fm) with fixed- d calculations for (b): G3RS2-3R and (d): V2m-3R.

shorter distances, $d \leq 2$ fm, the internal structure of the α clusters changes mainly because of the reduction of the 3D component, and the overlap with the frozen- α calculation shows the suppression of the two- α probability compared with the normalized $0s$ overlap.

C. Discussions for the two- α system

In order to clarify the roles of the tensor and short-range correlations in the two- α system, here we discuss the d dependence of the energy in more detail. We focus on the origin of the repulsive effects in the short-distance region ($d \leq 2$ fm) of the two- α system.

In Figs. 8, 9, and 10, we show the total energy and the contribution of each term of the Hamiltonian obtained by the and frozen- α calculations as well as those for the $0s$ state ($(0s)^4$ configuration for each α cluster). In order to stress the optimization of the correlated α cluster at each d , we call here the fixed- d calculation “optimized- α calculation”. We also show the contribution of the internal excitation energy of the α clusters caused by the changes in the internal structure and that of the external energy between α clusters defined in subsection II C. Energies are measured from the values at $d_{\max} = 8$ fm.

First, let us look into the energies of the $0s$ state; the conventional two- α cluster model without the NN correlations (lines “ $0s$ ” in Fig. 8). The d dependences of the two- α energy are similar in the G3RS2-3R (Fig. 8 (a)) and V2m-3R (Fig. 8 (d)) cases; mild repulsive effect in the long-distance region caused by the kinetic energy (Fig. 8 (b) and (e)) and the attractive effect in the middle-distance region owing to the central interaction (Fig. 8 (c) and (f)). These features are the same as V2: $0s$ in Fig. 6, but this attractive effect of the central interaction in G3RS2-3R and V2m-3R is smaller than in V2: $0s$ because of the weaker triplet-even part of the central interactions. As a result, the minimum point for the total energy disappears in the conventional $0s$ calculation for G3RS2-3R and V2m-3R.

Next, we compare energies of the frozen- α calculation (lines “frozen” in Fig. 8) with those for the $0s$ state (“ $0s$ ” in Fig. 8). The frozen- α calculation shows how the energy of the two- α system changes when they just come closer without the internal excitation (without the core polarization). The energy difference between these two shows the reflection of the high-momentum NN correlations in the ground state of ${}^4\text{He}$ to the two- α energy. The frozen- α calculation has the repulsive effect at short distances considerably higher than $0s$ (Fig. 8 (a) and (d)), which dominantly comes from the kinetic term (Fig. 8 (b) and (e)). Here the repulsive effect of the tensor term is also significantly large (Fig. 9 (a) and (d)). The energy differences at $d = 1$ fm are about 100 MeV for the kinetic term and about 30 MeV for the tensor term. These repulsive effects at short distances ($d \leq 2$ fm for the kinetic term and $d \leq 1$ fm for the tensor term) are attributed to the Pauli blocking effect for the high-momentum NN -

correlation in the 3D state. The repulsive effect of the tensor interaction is almost the same extent in G3RS2-3R and V2m-3R, whereas that of the kinetic term is slightly higher in G3RS2-3R than in V2m-3R because of larger mixing of high-momentum components in the correlated S -wave pair.

Then, we compare the results of the optimized- α calculation (lines “opt” in Fig. 8) with the frozen- α one (lines “frozen” in Fig. 8). The difference comes from the core polarization effect, *i.e.*, the internal structure change of the α cluster caused by the presence of another α cluster. In the optimized- α calculation, the total energy decreases because of the structure change in the $d \lesssim 2$ fm region, which is indeed seen in the significant reduction of the 3D component and enhancement of the $0s$ component (Table IV and Fig. 6). As already shown in the frozen- α calculation, the approaching α clusters strongly feel the repulsive effect coming from the kinetic term, but in the optimized- α calculation, the structure change allows to reduce the repulsive effect by suppressing the high-momentum NN -correlations mainly in the 3D channel. Moreover, in G3RS2, this D -state suppression also reduces the attractive effect of the central-even (mainly 3E) interaction, especially for its middle-range term ($\eta_{c,2} = 0.942$ fm), as shown in Fig. 10 (b).

The structure change of the α clusters approaching each other affects not only the internal excitation of the clusters but also the relative motion between them through the antisymmetrization effect for the nucleons in the two α clusters. To clearly distinguish these two effects, we separate the energy of the optimized- α calculation into the internal (lines “int”) and external (lines “ext”) parts as described previously (in subsection II C 5). Their d dependence is shown in Figs. 8, 9, and 10. Note that frozen- α does not contain the internal excitation energy by definition. Here the reduction of the kinetic energy in optimized- α compared with frozen- α is understood as the decrease of both the internal kinetic energy and external one due to the core polarization (Fig. 8 (b) and (e)); the reduction of the high-momentum correlations decreases both the internal and external kinetic energies. On the other hand, for the tensor term, the repulsive effect mainly comes from the large reduction of the 3D component in the internal part (Fig. 9 (b) and (e)). For the central interaction, the repulsive effect in the long-distance region of the central-odd term only weakly contributes to the external energy but not to the internal energy (Fig. 9 (c) and (f)) because its contribution to the binding energy of ${}^4\text{He}$ is quite small. These features are qualitatively similar in the G3RS2-3R and V2m-3R results.

However, for the central-even interaction, one can see a clear difference between G3RS2-3R and V2m-3R. The internal excitation provides significant repulsive effect in the region of $d \leq 2$ fm only in the case of G3RS2-3R (Fig. 9 (b) and (e)). In G3RS2-3R, this repulsive effect mainly comes from the middle-range ($\eta_{c,2} = 0.942$ fm) term particularly in the 3E channel (see Fig. 10 (b)).

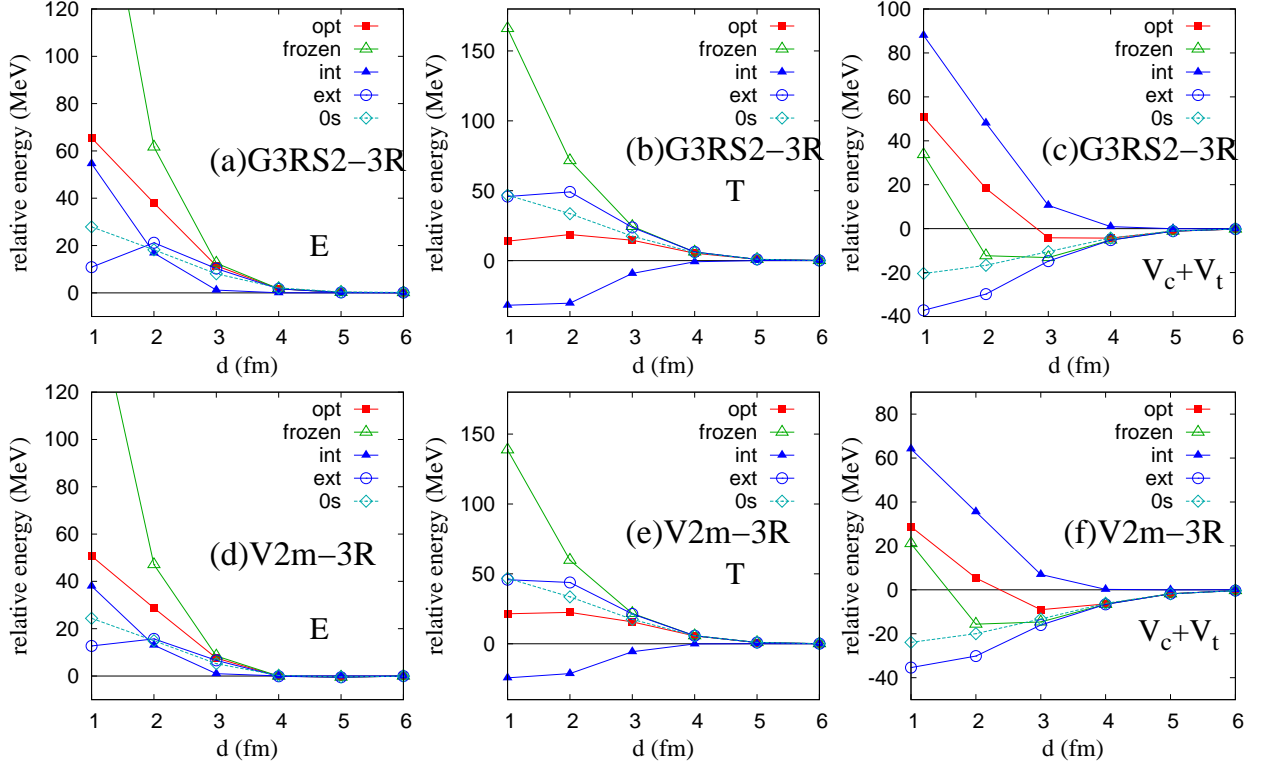


FIG. 8: (Color online) Energy for each component of the Hamiltonian of ${}^8\text{Be}$ obtained by the optimized- α (fixed- d) calculation (opt) and frozen- α calculation (frozen), and the conventional two- α cluster model with the $0s$ configuration ($0s$). The internal energy of α clusters (int) and external one between them (ext) are also shown. Upper panels: expectation values of the total energy (E , left), kinetic energy (T , middle), and the sum of the central and tensor interactions ($V_c + V_t$, right) for G3RS2-3R. Lower panels: those for V2m-3R. Relative energies measured from the values at d_{max} ($= 8$ fm) are plotted as functions of d .

As described in the previous section for ${}^4\text{He}$, in G3RS2-3R, the tensor correlation, *i.e.* the 3D component of the NN correlation, contributes also to the enhancement of the attraction coming from the middle-range of the central-even interaction through the 3S - 3D coupling. In the $d \leq 2$ fm region of the two- α system, not only the 3D component but also the correlated S -wave component is significantly reduced (see Fig. 6). This means that the D -state suppression by the Pauli blocking induces the reduction of the 3S component through the 3S - 3D coupling and results in the repulsive effect in the central-even interaction. Such an effect cannot be seen in V2m-3R, and this is a characteristic feature of G3RS2-3R containing the deep attraction (potential pocket) in the middle-range and the repulsion in the short-range of the central interaction, which are the origins of stronger repulsive effect in the $d \leq 2$ fm region of the α - α potential compared with V2m-3R.

VI. SUMMARY

In the present study, we aimed to describe the short-range correlation caused by the repulsive core of the cen-

tral interaction in addition to the tensor correlation. We applied AQCM-T to ${}^4\text{He}$ and ${}^8\text{Be}$ and in particular, we focused on the NN correlations in α clusters. We used the NN interactions including realistic ones containing a repulsive core for the central part. The adopted interactions are G3RS1-3R and G3RS2-3R, realistic interactions with the tensor term and short-range central core, V2m-3R, effective interaction with the tensor term but no short-range central core, and V2, effective interaction without the tensor nor short-range central core.

The binding energy and size of ${}^4\text{He}$ are reasonably reproduced with G3RS2-3R, V2m-3R, and V2 interactions, but the energy of each term of the Hamiltonian is different; G3RS2-3R and V2m-3R give higher kinetic energy and larger attraction of the potential energy than V2 because of the NN correlations. the tensor interaction gives significant contribution almost comparable to the central interaction. The energy of each term and D -state probability of ${}^4\text{He}$ obtained with G3RS2-3R and V2m-3R are similar, but some different features can be seen in the S -wave NN -correlations. The S -wave pair wave functions of G3RS2-3R show some suppression in the short-range ($r \lesssim 2$ fm) region and the enhancement of the peak in the middle-range ($r \sim 1$ fm) region, but those of V2m-3R

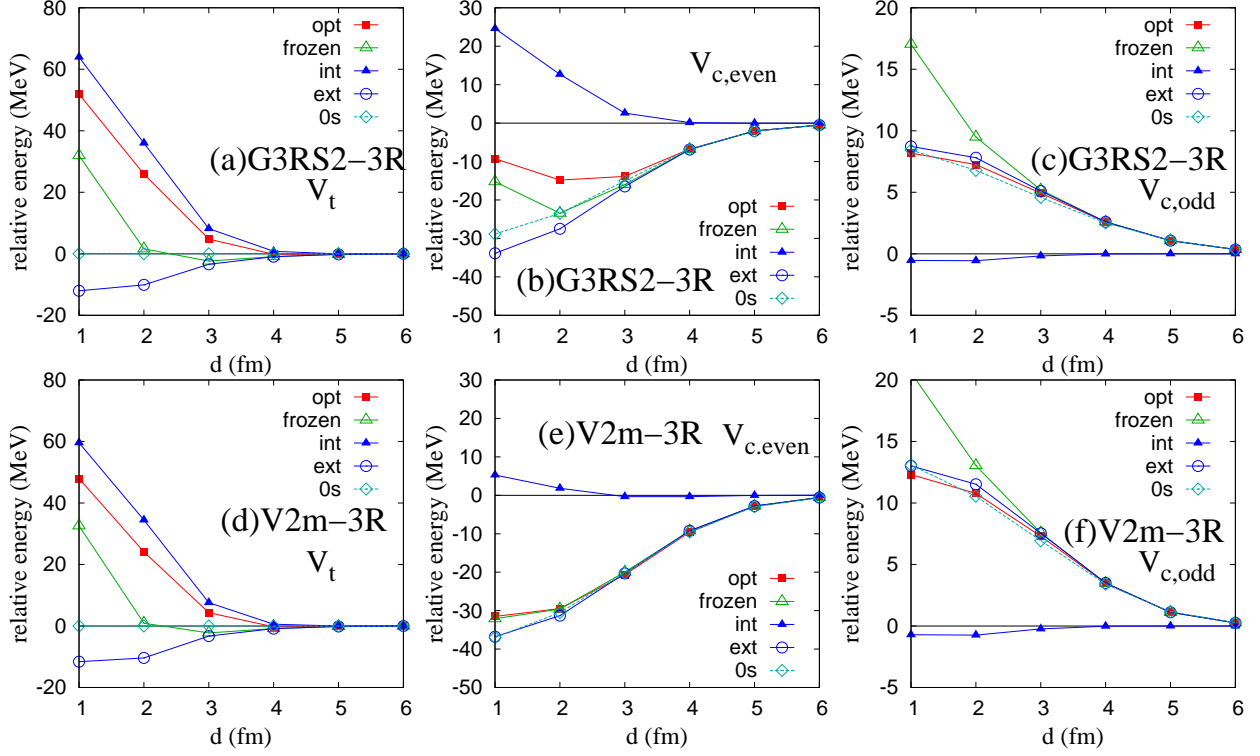


FIG. 9: (Color online) Same as Fig. 8 but for the tensor (V_t , left), central-even ($V_{c,even}$, middle), and central-odd ($V_{c,odd}$, right) interactions.

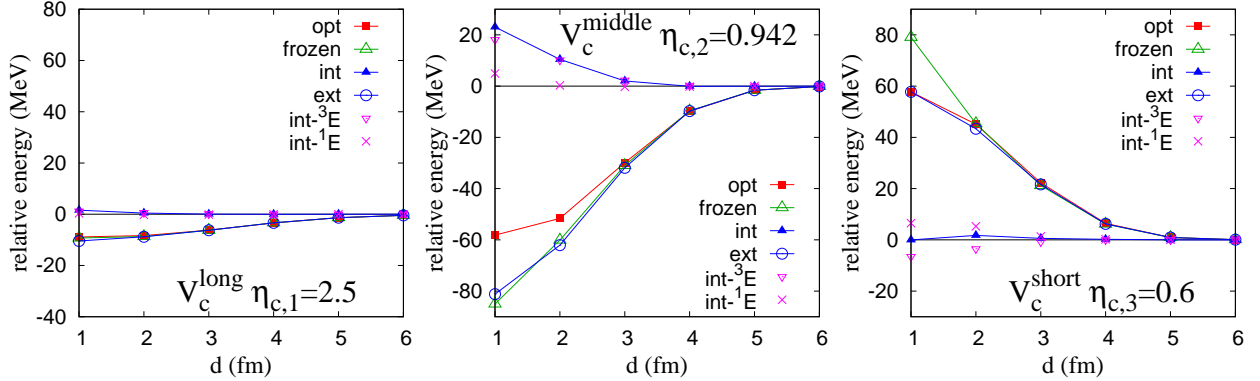


FIG. 10: (Color online) Same as Fig. 8 but for the long-range ($\eta_{c,1}=2.5$ fm), middle-range ($\eta_{c,2}=0.942$ fm), and short-range ($\eta_{c,3}=0.6$ fm) terms for the central-even part of G3RS2-3R are shown in the left, middle, and right, respectively. For the contribution of the internal energy, 3E ($int-^3E$) and 1E ($int-^1E$) parts are shown in addition to their sum (int).

do not show such features.

We also applied AQCM to the two- α cluster structure of ^8Be and compared the results of G3RS2-3R, V2m-3R, and V2, while paying attention to the roles of the NN correlations in the two- α potential. In the cases of G3RS2-3R and V2m-3R, as two α clusters approach each other, the attractive contribution of the tensor interaction is drastically reduced because the Pauli blocking effect between two α clusters suppresses the D -state

configuration in the α clusters. This tensor suppression gives a repulsive effect to the two- α system in the region of distance $d \gtrsim 2$ fm. This can be seen in G3RS2-3R and V2m-3R with the tensor terms but not in V2 without it. In G3RS2-3R, another repulsive effect is seen in the same d region, which comes from the reduction of the central-even interaction, but this effect originates from the same D -state suppression. Namely, the D -state suppression induces the decrease of the 3S component

through the ${}^3S\text{-}{}^3D$ coupling, which results in the reduction of the attractive effect of the central-even interaction in the middle-range region ($r \sim 1$ fm). Such repulsive effect for the contribution of the central-even interaction in $d \lesssim 2$ fm cannot be seen in V2m-3R without the repulsive core of the central interaction.

We have shown that the tensor effect can be taken into account by utilizing AQCM-T not only in ${}^4\text{He}$ but also in ${}^8\text{Be}$. The method can be applied to heavier nuclei and useful to clarify the interplay between the tensor correlation and appearance of the cluster structure in such nuclei as ${}^{12}\text{C}$ and ${}^{16}\text{O}$. Also, further renovation of the model, which is capable of utilizing interactions with

higher cores, is ongoing.

Acknowledgments

The computational calculations of this work were performed by using the supercomputer at Yukawa Institute for Theoretical Physics, Kyoto University. This work was supported by JSPS KAKENHI Grant Numbers 26400270 (Y. K-E.), 17K05440 (N. I.), 18J13400 (H. M.), and 18K03617 (Y. K-E.).

-
- [1] D. M. Brink, in *Proceedings of the International School of Physics "Enrico Fermi" Course XXXVI*, edited by C. Bloch (Academic, New York, 1966), p. 247.
- [2] Y. Fujiwara *et al.*, *Supple. of Prog. Theor. Phys.* **68**, 29 (1980).
- [3] F. Hoyle, D. N. F. Dunbar, W. A. Wenzel, and W. Whaling, *Phys. Rev.* **92**, 1095c (1953).
- [4] E. Uegaki, S. Okabe, Y. Abe, and H. Tanaka, *Prog. Theor. Phys.* **57**, 1262 (1977).
- [5] A. Tohsaki, H. Horiuchi, P. Schuck, and G. Röpke, *Phys. Rev. Lett.* **87**, 192501 (2001).
- [6] M. Sakai, I. Shimodaya, Y. Akaishi, J. Hiura, and H. Tanaka, *Supple. of Prog. Theor. Phys.* **56**, 32 (1974)
- [7] H. Kamada *et al.*, *Phys. Rev. C* **64**, 044001 (2001).
- [8] T. Myo, K. Katō, and K. Ikeda, *Prog. Theor. Phys.* **113**, 763 (2005).
- [9] M. Alvioli, C. Ciofi degli Atti, and H. Morita, *Phys. Rev. Lett.* **100**, 162503 (2008).
- [10] H. Feldmeier, W. Horiuchi, T. Neff, and Y. Suzuki, *Phys. Rev. C* **84**, 054003 (2011).
- [11] R. B. Wiringa, R. Schiavilla, S. C. Pieper, and J. Carlson, *Phys. Rev. C* **89**, 024305 (2014).
- [12] C. C. degli Atti, *Phys. Rep.* **590** 1 (2015).
- [13] M. Alvioli, C. C. degli Atti, and H. Morita, *Phys. Rev. C* **94**, 044309 (2016).
- [14] O. Hen, G. A. Miller, E. Piasetzky, and L. B. Weinstein, *Rev. Mod. Phys.* **89**, no. 4, 045002 (2017).
- [15] Y. Kanada-En'yo, H. Horiuchi, and A. Ono, *Phys. Rev. C* **52**, 628 (1995).
- [16] Y. Kanada-En'yo and H. Horiuchi, *Phys. Rev. C* **52**, 647 (1995).
- [17] Y. Kanada-En'yo and H. Horiuchi, *Supple. of Prog. Theor. Phys.* **142**, 205 (2001).
- [18] Y. Kanada-En'yo, M. Kimura, and A. Ono, *Prog. Theor. Exp. Phys.* **2012**, 01A202 (2012).
- [19] A. Doté, Y. Kanada-En'yo, H. Horiuchi, Y. Akaishi, and K. Ikeda, *Prog. Theor. Phys.* **115**, 1069 (2006).
- [20] T. Neff and H. Feldmeier, *Nucl. Phys.* **A738**, 357 (2004).
- [21] R. Roth, T. Neff, and H. Feldmeier, *Prog. Part. Nucl. Phys.* **65**, 50 (2010).
- [22] M. Chernykh, H. Feldmeier, T. Neff, P. von Neumann-Cosel, and A. Richter, *Phys. Rev. Lett.* **98**, 032501 (2007); *ibid* **105**, 022501 (2010).
- [23] N. Itagaki, H. Masui, M. Ito, and S. Aoyama, *Phys. Rev. C* **71**, 064307 (2005).
- [24] N. Itagaki, H. Masui, M. Ito, S. Aoyama, and K. Ikeda, *Phys. Rev. C* **73**, 034310 (2006).
- [25] H. Masui and N. Itagaki, *Phys. Rev. C* **75**, 054309 (2007).
- [26] T. Yoshida, N. Itagaki, and T. Otsuka, *Phys. Rev. C* **79**, 034308 (2009).
- [27] N. Itagaki, J. Cseh, and M. Płoszajczak, *Phys. Rev. C* **83**, 014302 (2011).
- [28] T. Suhara, N. Itagaki, J. Cseh, and M. Płoszajczak, *Phys. Rev. C* **87**, 054334 (2013).
- [29] T. Suhara and Y. Kanada-En'yo, *Phys. Rev. C* **91**, 024315 (2015).
- [30] N. Itagaki, H. Matsuno, and T. Suhara, *Prog. Theor. Exp. Phys.* **2016**, 093D01 (2016).
- [31] N. Itagaki, *Phys. Rev. C* **94**, 064324 (2016).
- [32] H. Matsuno, N. Itagaki, T. Ichikawa, Y. Yoshida, and Y. Kanada-En'yo, *Prog. Theor. Exp. Phys.* **2017**, 063D01 (2017).
- [33] H. Matsuno and N. Itagaki, *Prog. Theor. Exp. Phys.* **2017**, 123D05 (2017).
- [34] N. Itagaki and A. Tohsaki, *Phys. Rev. C* **97**, 014307 (2018).
- [35] N. Itagaki and A. Tohsaki, *Phys. Rev. C* **97**, 014304 (2018).
- [36] T. Myo, H. Toki, K. Ikeda, H. Horiuchi, T. Suhara, M. Lyu, M. Isaka, and T. Yamada, *Prog. Theor. Exp. Phys.* **2017**, 111D01 (2017).
- [37] T. Myo, *Prog. Theor. Exp. Phys.* **2018**, 031D01 (2018).
- [38] H. Matsuno, Y. Kanada-En'yo, and N. Itagaki, *arXiv.1805.10087*.
- [39] H. Bandō, S. Nagata, and Y. Yamamoto, *Prog. Theor. Phys.* **44**, 646 (1970).
- [40] R. B. Wiringa, Steven C. Pieper, J. Carlson, and V. R. Pandharipande, *Phys. Rev. C* **62**, 014001 (2000).
- [41] Y. Yamamoto, T. Togashi, and K. Katō, *Prog. Theor. Phys.* **44**, 646 (2010).
- [42] K. Horii, H. Toki, T. Myo, and K. Ikeda, *Prog. Theor. Phys.* **127**, 1019 (2012).
- [43] R. Tamagaki, *Prog. Theor. Phys.* **39**, 91 (1968).
- [44] A. B. Volkov, *Nucl. Phys.* **74**, 33 (1965).
- [45] D. M. Brink and E. Boeker, *Nucl. Phys. A* **91**, 1 (1967).
- [46] I. Angeli and K. P. Marinova, *At. Data Nucl. Data Tables* **99**, 69 (2013).